

EXTENDED STEFAN PROBLEM FOR SOLIDIFICATION OF BINARY ALLOYS IN A FINITE PLANAR DOMAIN*

FERRAN BROSÀ PLANELLA[†], COLIN P. PLEASE[†], AND ROBERT A. VAN GORDER[‡]

Abstract. We consider the extended Stefan problem for the solidification of a binary alloy in a finite one-dimensional domain accounting for constitutional supercooling. In this problem, solidification fronts start from each boundary and move inward toward one another. We perform an asymptotic analysis of the problem in the limit of large Lewis number, which allows us to identify four important temporal regimes corresponding to distinct behaviors in the solidification process. We find that, for small time, the two solidification fronts are initially far from one another, and move in a self-similar manner toward the interior of the domain. However, when the fronts are sufficiently close, expelled impurities (which diffuse into, and build up within, the liquid phase between the two fronts) increase in concentration, inducing supercooling and thereby slowing the motion of the fronts. For large time, the system tends to its minimum temperature (corresponding to the boundary of the finite domain), with the concentration of impurities following in thermodynamic equilibrium. Asymptotic solutions in each spatiotemporal region are obtained and then matched to neighboring temporal regimes and spatial layers, and by matching we obtain global asymptotic solutions to the extended Stefan problem. We compare our asymptotic solutions to numerical simulations of the full problem obtained by a finite volume method, and the respective solutions show excellent agreement. We also compare our asymptotic solutions to real experimental data arising from the casting process for molten metallurgical grade silicon, with our analysis highlighting the role of supercooling in the solidification of binary alloys appearing in such applications.

Key words. two-phase Stefan problem, solidification of binary alloys, matched asymptotic analysis

AMS subject classifications. 80A22, 35R37, 34E10, 80A20

DOI. 10.1137/18M118699X

1. Introduction. The process of solidification arises in a variety of applications, from freezing water to metallurgy. Many solidification processes are modeled using Stefan problems. Stefan problems, first posed in [21] and generalized to both solid and liquid phases in [35], have been extended to many applications [31]. Closed-form analytical solutions for Stefan problem are obtained only in the simplest cases. Self-similar solutions can be found for the two-phase Stefan problem in semi-infinite domains, and in some cases they can be extended to include constitutional supercooling [31]. Although self-similar solutions for the supercooled problem may be unstable [4], they still provide valuable insight on the dynamics of the system. However, in the physically interesting cases when the problem domain is finite, self-similar solutions may no longer exist.

*Received by the editors May 14, 2018; accepted for publication (in revised form) April 4, 2019; published electronically June 4, 2019.

<http://www.siam.org/journals/siap/79-3/M118699.html>

Funding: This work was supported by the EPSRC Centre for Doctoral Training in Industrially Focused Mathematical Modeling through grant EP/L015803/1. The work of the first author was supported by Elkem ASA.

[†]Mathematical Institute, University of Oxford, Andrew Wiles Building, Radcliffe Observatory Quarter, Woodstock Road, Oxford, OX2 6GG, United Kingdom (Ferran.BrosaPlanella@maths.ox.ac.uk, please@maths.ox.ac.uk).

[‡]Mathematical Institute, University of Oxford, Andrew Wiles Building, Radcliffe Observatory Quarter, Woodstock Road, Oxford, OX2 6GG, United Kingdom, and Department of Mathematics and Statistics, University of Otago, P.O. Box 56, Dunedin 9054, New Zealand (rvangorder@maths.otago.ac.nz).

Much attention has been devoted to finding asymptotic approximations for the inward solidification of many different geometries where the liquid is initially at the melting temperature; such problems can at times be formulated as one-phase Stefan problems. A common asymptotic limit to consider is that where the Stefan number is large, corresponding to the situation where latent heat dominates, with planar two-dimensional geometries, such as a half-space [40] or a corner [18], cylindrical and spherical geometries [30, 33, 36], and arbitrary two-dimensional [25] and three-dimensional [26] geometries having been considered. Small-time behavior [8, 13, 14] and end-time behavior (near the end of the solidification process) [25, 26, 30, 33, 36] have been studied for the one-phase problem. In addition to asymptotic analysis, various numerical approaches for solving one-phase Stefan problems have been considered [1, 6, 7, 22, 24, 32, 37].

Despite their relevance to solidification problems, two-phase Stefan problems in finite domains have received less attention than their one-phase counterparts. Kucera and Hill [20] extended their previous small-time analysis to the two-phase problem, and compared their analytical solution with that found in [17]. They also employed the enthalpy method [39] to the two-phase problem. The two-phase Stefan problem in spheres was considered in [27] including a rigorous asymptotic analysis and numerical simulations via the enthalpy method. The more complicated two-phase Stefan problem, arising in the inward solidification of binary alloys, has received even less attention. When constitutional supercooling is included in the model, the analysis becomes more difficult, as now the problem consists of heat and mass transport problems coupled by constitutional supercooling conditions. Feltham and Garside [10] studied small time and large Stefan number behavior from the extended two-phase problem for binary alloys, in the regime where supercooling is small enough to decouple the heat and mass problems. This reduces the problem to a classic two-phase Stefan problem for the temperature (which is solved first) and a diffusion problem for concentration in a shrinking domain that can be solved once the position of the interface is known. The analytical results give a reasonable agreement with numerical simulations of the full problem, except that the analytical solution concentration in the liquid exhibits a nonphysical discontinuity in the flux at the origin. The inward solidification of a binary alloy sphere has also been considered in [43], but the authors considered the particular case where the liquid is a well-mixed liquid and thus the concentration and temperature profiles are uniform in space. Hence, their model is equivalent to a one-phase Stefan problem with a supercooling condition that depends on the position of the interface.

One physical application of the extended two-phase Stefan problem in finite domains is to the solidification of metallurgical grade silicon, which is composed of nearly 99% silicon, while the remaining fraction consists of impurities. The molten silicon is poured into iron moulds and left to solidify by the heat exchange with the environment. As the thickness of the cast is small in comparison with the width, the solidification mainly involves two fronts, one starting at the bottom and one at the top of the cast, which move toward one another until they meet at the center of the cast. During the solidification process, the impurities are mostly rejected from the solid phase into the liquid, within which they diffuse. The role of the impurities is crucial, as they cause constitutional supercooling in the liquid and therefore have an impact on the solidification front. For the silicon casting, a semi-infinite geometry can be useful to model the early stages of the process when the two solidification fronts are far from each other. However, such a formulation is no longer valid when the two fronts approach one another. Previous work showed good agreement between the

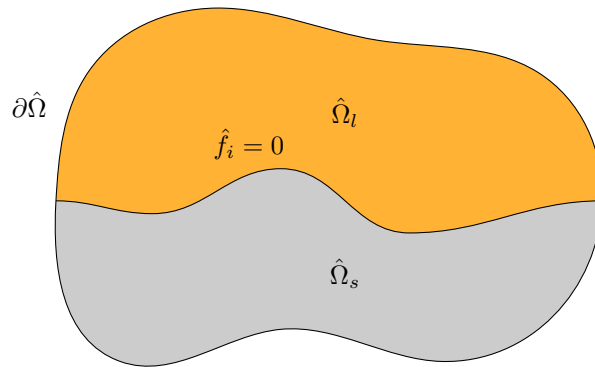


FIG. 1. Diagram of a general domain defined as $\hat{\Omega} = \hat{\Omega}_s \cup \hat{\Omega}_l \cup \{\hat{f}_i = 0\} \cup \partial\hat{\Omega}$, where $\hat{\Omega}_s$ denotes the solid phase and $\hat{\Omega}_l$ denotes the liquid phase. The boundary between both domains is assumed to be sharp, and it is given by an implicit relation $\hat{f}_i = 0$. The external boundary is given by $\partial\hat{\Omega}$.

classic two-phase Stefan problem and experimental data [3]. However, the distribution of impurities was neglected in this model, and therefore the model did not account for supercooling, which may modify the final-time dynamics when the solidification fronts approach.

In the present paper, we solve the extended Stefan problem with constitutional supercooling in a finite planar domain using matched asymptotics, exploiting the fact that the Lewis number is large. While relatively simple, the one-dimensional planar geometry is still quite relevant to model a silicon cast. Our results extend the analysis of the solidification of a slab presented in [10] to include supercooling that couples the heat and mass problems, and we shall also consider all time scales of the problem. The outline of the article is the following. In section 2 we present the general model for the solidification of a binary alloy, and nondimensionalize it. From here we derive the planar geometry model. In section 3 we perform an asymptotic analysis determining the leading order approximation to the solutions for the entire problem at various time scales, and use these to assemble matched asymptotic solutions to the problem. In section 4, we compare the matched asymptotic solutions to numerical simulations of the full problem obtained with a finite volume method, and also to real experimental data obtained from silicon casting experiments. We discuss our results in section 5.

2. General model for the solidification of a binary alloy. Consider a domain $\hat{\Omega} \in \mathbb{R}^n$ which is split into two subdomains: the solid phase $\hat{\Omega}_s$ (sometimes called the crystal phase in the literature) and the liquid phase $\hat{\Omega}_l$ (sometimes called the melt phase in the literature). These two regions are separated by a sharp interface defined by the $(n - 1)$ -dimensional surface defined implicitly by $\hat{f}_i = 0$, while they have an outer boundary $\partial\hat{\Omega}$. Then, $\hat{\Omega} = \hat{\Omega}_s \cup \hat{\Omega}_l \cup \{\hat{f}_i = 0\} \cup \partial\hat{\Omega}$, and the intersection between any of the subsets is empty for any time $\hat{t} > 0$. A diagram of our problem is shown in Figure 1. Although the two domains $\hat{\Omega}_l$ and $\hat{\Omega}_s$ are shown as connected domains, this is not a requirement. Furthermore, the form of the subdomains $\hat{\Omega}_s$ and $\hat{\Omega}_l$ vary as the liquid solidifies.

We model temperature \hat{T}_s or \hat{T}_l and concentration of impurities \hat{c}_s or \hat{c}_l , respectively, in each subdomain, while also keeping track of the time evolution of the interface \hat{f}_i . We assume conservation of mass and energy in each phase and across the moving interface, and couple the phases under an assumption of constitutional

supercooling. The effects of constitutional supercooling are reflected in phase diagrams which become rather complex when more than two components are considered [5, 19]. We assume all impurities constitute a single phase, resulting in a binary phase problem between the pure material and the impurities. We assume that the relation between the impurity concentration and the temperature on both the liquidus and the solidus is linear. We take the Boussinesq approximation (see [15, 42]), assuming that the change in density affects the thermal diffusivity but it does not induce advection in the liquid. We assume the difference in density between the solid and liquid phases is small and neglect the flow generated at the interface due to the expansion of the material. Therefore, we assume that the solid and liquid are stationary so heat and mass transport are driven only by diffusion.

We impose boundary conditions at the outer boundary $\partial\hat{\Omega}$, which corresponds to the wall of the mould. In particular, we prescribe a no-flux condition for the concentration of impurities (as they cannot flow through the mould), as well as a fixed uniform temperature. A more realistic approach could be taken by using a heat exchange condition (as done in [3, 13]). However, in the limit where the heat exchange coefficient is large, this condition can be approximated by a Dirichlet boundary condition. We assume that the entire domain is liquid, with homogeneous temperature and concentration of impurities, at the initial time.

2.1. Dimensional model. With all these assumptions, we can proceed to write the dimensional model down. For the solid phase, defined as $\hat{\mathbf{x}} \in \hat{\Omega}_s$, the equations read

$$(2.1a) \quad \frac{\partial \hat{c}_s}{\partial \hat{t}} = \nabla \cdot (D_s \nabla \hat{c}_s) \quad \text{and} \quad \rho_s c_{ps} \frac{\partial \hat{T}_s}{\partial \hat{t}} = \nabla \cdot (k_s \nabla \hat{T}_s),$$

where $\hat{c}_s(\hat{\mathbf{x}}, \hat{t})$ is the concentration of impurities (in mass per unit volume), $\hat{T}_s(\hat{\mathbf{x}}, \hat{t})$ is the temperature, D_s is the diffusivity of impurities, ρ_s is the density, c_{ps} is the specific heat, and k_s is the thermal conductivity; all of these quantities are defined in the solid phase.

In the liquid phase, defined as $\hat{\mathbf{x}} \in \hat{\Omega}_l$, the equations are

$$(2.1b) \quad \frac{\partial \hat{c}_l}{\partial \hat{t}} = \nabla \cdot (D_l \nabla \hat{c}_l) \quad \text{and} \quad \rho_l c_{pl} \frac{\partial \hat{T}_l}{\partial \hat{t}} = \nabla \cdot (k_l \nabla \hat{T}_l),$$

where $\hat{c}_l(\hat{\mathbf{x}}, \hat{t})$, $\hat{T}_l(\hat{\mathbf{x}}, \hat{t})$, D_l , ρ_l , c_{pl} , and k_l are as above, only defined in the liquid phase.

The conditions at the interface $\hat{f}_i = 0$ are

$$(2.1c) \quad \hat{T}_s = \hat{T}_l, \quad \hat{c}_s = -\alpha_s(\hat{T}_s - T_{m0}), \quad \hat{c}_l = -\alpha_l(\hat{T}_l - T_{m0}),$$

$$(2.1d) \quad \rho_s L \frac{\partial \hat{f}_i}{\partial \hat{t}} = -k_s \nabla \hat{T}_s \cdot \nabla \hat{f}_i + k_l \nabla \hat{T}_l \cdot \nabla \hat{f}_i, \quad (\hat{c}_l - \hat{c}_s) \frac{\partial \hat{f}_i}{\partial \hat{t}} = -D_s \nabla \hat{c}_s \cdot \nabla \hat{f}_i + D_l \nabla \hat{c}_l \cdot \nabla \hat{f}_i,$$

where T_{m0} is the melting temperature for the pure material, L is the latent heat of solidification, and α_s and α_l are the slopes of the liquidus and solidus curves, respectively, which as shown in Figure 2 are assumed to be linear.

The boundary conditions are given by

$$(2.1e) \quad \frac{\partial \hat{c}_s}{\partial \hat{n}} = 0 \quad \text{and} \quad \hat{T}_s = T_c \quad \text{at} \quad \hat{\mathbf{x}} \in \partial\hat{\Omega},$$

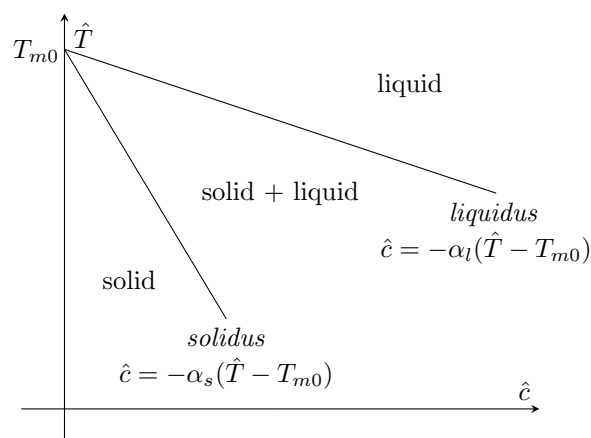


FIG. 2. Sketch of the linearized phase diagram that gives the thermodynamic equilibrium conditions that couple temperature and concentration of impurities at the interface.

where T_c is the uniform temperature at the boundary while $\frac{\partial}{\partial \hat{n}}$ is the normal derivative to the interface. Notice that we only prescribe the boundary conditions for the solid phase: we assume the boundary temperature is below the initial liquidus temperature so a layer of solid is formed around the boundary as soon as the process begins.

The initial conditions of the system are

$$(2.1f) \quad \hat{c}_l = c_0, \quad \hat{T}_l = T_0, \quad \hat{\Omega}_s = \emptyset, \quad \text{and} \quad \{f_i = 0\} = \partial\hat{\Omega} \quad \text{at} \quad \hat{t} = 0,$$

where T_0 and c_0 are the initial temperature and concentration (measured as mass of impurities per unit volume of melt) of the melt, respectively. We assume that the entire domain is initially liquid, and therefore do not impose initial conditions for the solid phase.

As an observation, in (2.1d) we have used the definitions of the normal velocity u_n and the normal vector \mathbf{n} given by

$$(2.2) \quad u_n = -\frac{1}{\|\nabla f_i\|} \frac{\partial f_i}{\partial t} \quad \text{and} \quad \mathbf{n} = \frac{1}{\|\nabla f_i\|} \nabla f_i,$$

which can be found in [28, 34].

2.2. Nondimensional model. We now proceed to nondimensionalize the model (2.1). We choose the scalings $\hat{t} = \frac{R^2}{\kappa_l} t$, $\hat{\mathbf{x}} = R\mathbf{x}$, $\hat{c} = \Delta c c$, $\hat{T} = \Delta T T + T_{m0}$, $\hat{\Omega}_s = R\Omega_s$, $\hat{\Omega}_l = R\Omega_l$, $\hat{f}_i = Rf_i$, $\partial\hat{\Omega} = R\partial\Omega$, where R is the scaling of the spatial coordinates, ΔT the scaling of temperature, T_{m0} the melting temperature for pure silicon, and Δc the scaling of concentration. We choose $\Delta T = T_{m0} - T_c$ and $\Delta c = \rho_l$. We assume that the material properties are homogeneous in each phase, so they can be pulled out of the divergences in (2.1).

We define the dimensionless parameters $\text{St} = \frac{\Delta T c_{pl}}{L}$, $\rho = \frac{\rho_s}{\rho_l}$, $k = \frac{k_s}{k_l}$, $c_p = \frac{c_{ps}}{c_{pl}}$, $\kappa = \frac{\kappa_s}{\kappa_l}$, $\text{Le} = \frac{\kappa_l}{D_l}$, $D = \frac{D_s}{D_l}$, $\alpha = \frac{\alpha_s}{\alpha_l}$, $m_s = \alpha_s \frac{\Delta T}{\Delta c}$, $m_l = \alpha_l \frac{\Delta T}{\Delta c}$, where κ_j is the thermal

diffusivity of each phase defined as $\kappa_j = \frac{k_j}{\rho_j c_{pj}}$. The dimensional model (2.1) becomes

$$(2.3a) \quad \frac{\partial c_s}{\partial t} = \frac{D}{Le} \nabla^2 c_s \quad \text{and} \quad \frac{\partial T_s}{\partial t} = \kappa \nabla^2 T_s,$$

$$(2.3b) \quad \frac{\partial c_l}{\partial t} = \frac{1}{Le} \nabla^2 c_l \quad \text{and} \quad \frac{\partial T_l}{\partial t} = \nabla^2 T_l,$$

$$(2.3c) \quad T_s = T_l, \quad c_s = -m_s T_s = \alpha c_l, \quad c_l = -m_l T_l,$$

$$(2.3d) \quad \frac{\rho}{St} \frac{\partial f_i}{\partial t} = -k \nabla T_s \cdot \nabla f_i + \nabla T_l \cdot \nabla f_i, \quad (1 - \alpha) c_l \frac{\partial f_i}{\partial t} = -\frac{D}{Le} \nabla c_s \cdot \nabla f_i + \frac{1}{Le} \nabla c_l \cdot \nabla f_i,$$

at the interface ($f_i = 0$),

$$(2.3e) \quad \frac{\partial c_s}{\partial n} = 0 \quad \text{and} \quad T_s = \frac{T_c - T_{m0}}{\Delta T} = -1 \quad \text{at } \mathbf{x} \in \partial\Omega,$$

$$(2.3f) \quad c_l = \frac{c_0}{\Delta c}, \quad T_l = \frac{T_0 - T_{m0}}{\Delta T}, \quad \Omega_s = \emptyset, \quad \text{and} \quad f_i = \partial\Omega \quad \text{at } t = 0.$$

Notice that we have used the definition of c_s in (2.3c) to rearrange the left-hand side of the second equation in (2.3d).

2.3. Asymptotic scalings. We assume a small diffusivity of impurities in the liquid, even smaller diffusivity in the solid, small initial temperature and concentration, small constitutional supercooling, and almost complete rejection of impurities from the solid phase. We define the small parameter $\epsilon = \frac{1}{Le} \ll 1$, and with this we rescale the model parameters as $D = \epsilon \hat{D}$, $m_l = \frac{\hat{m}_l}{\epsilon}$, $\alpha = \epsilon \hat{\alpha}$, $\frac{c_0}{\Delta c} = \epsilon \hat{c}_0$, $\frac{T_0 - T_{m0}}{\Delta T} = \epsilon \hat{T}_0$, where \hat{D} , \hat{m}_l , $\hat{\alpha}$, \hat{c}_0 , and \hat{T}_0 are of order one. These scalings are motivated by the typical parameter values for the solidification of metallurgical grade silicon. We rewrite (2.3) in terms of this scaling with ϵ , obtaining

$$(2.4a) \quad \frac{\partial c_s}{\partial t} = \epsilon^2 \hat{D} \nabla^2 c_s \quad \text{and} \quad \frac{\partial T_s}{\partial t} = \kappa \nabla^2 T_s \quad \text{in } \mathbf{x} \in \Omega_s,$$

$$(2.4b) \quad \frac{\partial c_l}{\partial t} = \epsilon \nabla^2 c_l \quad \text{and} \quad \frac{\partial T_l}{\partial t} = \nabla^2 T_l \quad \text{in } \mathbf{x} \in \Omega_l,$$

$$(2.4c) \quad T_s = T_l, \quad c_s = \epsilon \hat{\alpha} c_l, \quad \epsilon c_l = -\hat{m}_l T_l,$$

$$(2.4d) \quad \frac{\rho}{St} \frac{\partial f_i}{\partial t} = -k \nabla T_s \cdot \nabla f_i + \nabla T_l \cdot \nabla f_i, \quad (1 - \epsilon \hat{\alpha}) c_l \frac{\partial f_i}{\partial t} = -\epsilon^2 \hat{D} \nabla c_s \cdot \nabla f_i + \epsilon \nabla c_l \cdot \nabla f_i$$

at the interface ($f_i = 0$),

$$(2.4e) \quad \frac{\partial c_s}{\partial n} = 0 \quad \text{and} \quad T_s = -1 \quad \text{at } \mathbf{x} \in \partial\Omega,$$

$$(2.4f) \quad c_l = \epsilon \hat{c}_0, \quad T_l = \epsilon \hat{T}_0, \quad \Omega_s = \emptyset, \quad \text{and} \quad \{f_i = 0\} = \partial\Omega \quad \text{at } t = 0.$$

2.4. Nondimensional model for planar geometry. The geometry of the planar solidification problem consists of a finite slab, initially a liquid with homogeneous temperature and concentration of impurities, which is cooled from both ends at a uniform temperature which is constant in time. For simplicity, we assume the problem to be symmetric, therefore we need only consider half of the domain, provided we impose symmetry conditions at the origin. A diagram of the planar geometry is shown in Figure 3.

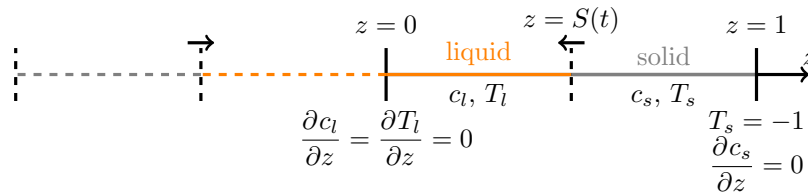


FIG. 3. Diagram of the inward solidification problem of a finite slab. We assume that the problem is symmetric with respect to $z = 0$, so we consider the problem only in the region $0 \leq z \leq 1$ and impose symmetry conditions at the origin.

We take z to be the dimensionless spatial coordinate so that the problem is defined in the domain $0 \leq z \leq 1$, while the position of the interface is given by $f_i = z - S(t)$. The nondimensional model (2.4) becomes

$$(2.5a) \quad \frac{\partial c_s}{\partial t} = \epsilon^2 \hat{D} \frac{\partial^2 c_s}{\partial z^2}, \quad \frac{\partial T_s}{\partial t} = \kappa \frac{\partial^2 T_s}{\partial z^2} \quad \text{on } z > S(t),$$

$$(2.5b) \quad \frac{\partial c_l}{\partial t} = \epsilon \frac{\partial^2 c_l}{\partial z^2}, \quad \frac{\partial T_l}{\partial t} = \frac{\partial^2 T_l}{\partial z^2} \quad \text{on } z < S(t),$$

$$(2.5c) \quad T_s = T_l, \quad c_s = \epsilon \hat{\alpha} c_l, \quad \epsilon c_l = -\hat{m}_l T_l,$$

$$(2.5d) \quad \frac{\rho}{St} \frac{dS}{dt} = k \frac{\partial T_s}{\partial z} - \frac{\partial T_l}{\partial z}, \quad (1 - \epsilon \hat{\alpha}) c_l \frac{dS}{dt} = \epsilon^2 \hat{D} \frac{\partial c_s}{\partial z} - \epsilon \frac{\partial c_l}{\partial z}$$

at the interface ($z = S(t)$),

$$(2.5e) \quad \frac{\partial c_l}{\partial z} = 0 \quad \text{and} \quad \frac{\partial T_l}{\partial z} = 0 \quad \text{at } z = 0,$$

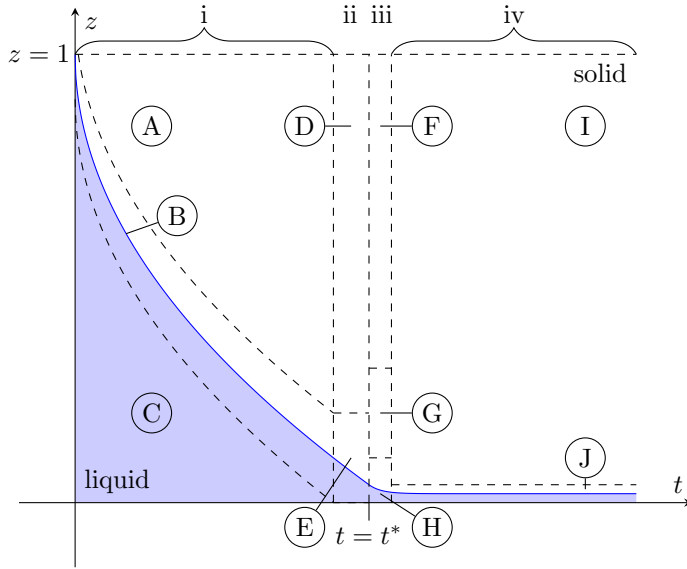
$$(2.5f) \quad \frac{\partial c_s}{\partial z} = 0 \quad \text{and} \quad T_s = -1 \quad \text{at } z = 1,$$

$$(2.5g) \quad c_l = \epsilon \hat{c}_0, \quad T_l = \epsilon \hat{T}_0, \quad \text{and} \quad S = 1 \quad \text{at } t = 0.$$

As exact solutions are seemingly not possible, in section 3, we perform an asymptotic analysis to find solutions of the system (2.5). These asymptotic solutions are then compared with numerical simulations and real experimental data in section 4.

3. Asymptotic analysis. The asymptotic analysis of the problem in the limit $\epsilon \rightarrow 0$ reveals four distinct time regimes in the problem, and each regime is composed of different space layers. We identify ten layers overall, with a schematic diagram and list of relevant scalings shown in Figure 4. Notice that we use hats for the position of the interface and the temperature and concentration fields whenever they are rescaled.

These scalings are primarily picked by the physics. At the beginning of the process, in what we call regime i, we expect to see diffusion of both heat and impurities, but, due to the disparity in diffusive length scales, we need to introduce an inner layer of size $\mathcal{O}(\epsilon)$ around the interface (named layer B) to capture the rejection and transport of impurities, while heat diffusion is observed in the outer layers (A and C). This regime holds until the interface is within a distance $\mathcal{O}(\epsilon)$ from the origin, as now the outer layer in the liquid vanishes and the inner layer around the interface needs to account for the symmetry conditions at the origin. This sets the scalings for S and z , and thus defines the two layers (D and E) in regime ii. The time scale arises from balancing the Stefan condition that appears in the inner layer E, as we need a time scale that allows us to observe the motion of the solidification front. We find that



		t	z	S	c_s	c_l	T_s	T_l
Regime i	A	t	z	S	$\epsilon \hat{c}_s$	-	T_s	-
	B	t	$S(t) + \epsilon Z$	S	$\epsilon \hat{c}_s$	c_l	$\epsilon \hat{T}_s$	$\epsilon \hat{T}_l$
	C	t	z	S	-	$\epsilon \hat{c}_l$	-	$\epsilon \hat{T}_l$
Regime ii	D	$t^* + \epsilon \tau$	z	$\epsilon \hat{S}$	$\epsilon \hat{c}_s$	-	T_s	-
	E	$t^* + \epsilon \tau$	ϵZ	$\epsilon \hat{S}$	$\epsilon \hat{c}_s$	c_l	$\epsilon \hat{T}_s$	$\epsilon \hat{T}_l$
Regime iii	F	$t^* + \epsilon \tau^* + \epsilon^{\frac{4}{3}} \theta$	z	$\epsilon^{\frac{4}{3}} \hat{S}$	$\epsilon \hat{c}_s$	-	T_s	-
	G	$t^* + \epsilon \tau^* + \epsilon^{\frac{4}{3}} \theta$	$\epsilon^{\frac{2}{3}} \xi$	$\epsilon^{\frac{4}{3}} \hat{S}$	$\epsilon \hat{c}_s$	-	$\epsilon^{\frac{2}{3}} \hat{T}_s$	-
	H	$t^* + \epsilon \tau^* + \epsilon^{\frac{4}{3}} \theta$	$\epsilon^{\frac{4}{3}} Z$	$\epsilon^{\frac{4}{3}} \hat{S}$	$\epsilon^{\frac{2}{3}} \hat{c}_s$	$\epsilon^{-\frac{1}{3}} \hat{c}_l$	$\epsilon^{\frac{2}{3}} \hat{T}_s$	$\epsilon^{\frac{2}{3}} \hat{T}_l$
Regime iv	I	t	z	$\epsilon^2 \hat{S}$	$\epsilon \hat{c}_s$	-	T_s	-
	J	t	$\epsilon^2 Z$	$\epsilon^2 \hat{S}$	c_s	$\epsilon^{-1} \hat{c}_l$	T_s	T_l

FIG. 4. Sketch of the regimes and layers of the process. The sketch shows the evolution of the interface, $S(t)$, in time, so the area above (in white) is the solid phase and the area below (in blue) is the liquid phase. The four regimes identified with lower case Roman numerals are the behaviors at different times. In each regime, we consider various layers which are labeled with upper case letters. The scalings in each layer are shown in the table. The variables τ and θ are the time variables at different regimes and the variables ξ and Z are the space variables in the intermediate and inner layers of each regime, respectively. For temperature, concentration, and the position of the interface we use hats whenever they are rescaled.

regime ii is valid until the inner layer E vanishes because the leading order interface position becomes zero. Therefore, we need to study a new regime, which we call regime iii. We expect this regime to be a transition between regimes ii and iv, which is discussed later. This transition is driven by the thermal problem in the solid, with the constitutional supercooling effect due to the buildup of impurities in the liquid phase. To capture this problem, we need to introduce the following layer structure: an outer layer F in the solid where both temperature and concentration fields remain constant, an intermediate layer G in the solid where we observe heat diffusion, and an inner layer H that captures the motion of the interface and thus accounts for the interface conditions. A balance of the relevant terms gives the scalings reproduced in Figure 4. Finally, we need to consider a last regime that holds up to $t \rightarrow +\infty$.

This is regime iv, in which we observe the temperature in the solid to decay down to the minimum temperature of the system, which corresponds to the temperature at the boundary $z = 1$. This behavior is observed in the outer layer I, but we need to account for the inner layer J to capture the moving boundary and the liquid region.

Notice that, according to the scalings in Figure 4, we have concentrations in the liquid phase of $\mathcal{O}(\epsilon^{-\frac{1}{3}})$ and $\mathcal{O}(\epsilon^{-1})$ which are not physical. As we discuss later, regimes iii and iv are not physical because some of the modeling assumptions, such as the linear phase diagram, no longer hold. This is related to the fact that, according to the model, the solidification process never finishes and therefore we always end up with a thin layer of liquid, which obviously does not agree with experimental observations. However, from the mathematical point of view, regimes iii and iv are relevant to provide a full picture of (2.5) for $t \in [0, +\infty)$.

In what follows, we find asymptotic solutions in each region, and then match them to construct solutions valid over the whole problem domain.

3.1. Asymptotic solutions in regime i. We start by considering the behavior at the beginning of the solidification process, described by regime i. In this regime, the interface is far from the origin and we distinguish three space layers. The outer layer A in the solid, the inner layer B around the solidification front which comprises both phases, and the outer layer C in the liquid. We start solving the equations for each layer and then proceed to match the layers between them in order to fully determine the solutions.

3.1.1. Layer A. The first layer we study in this regime is the outer layer in the solid phase: layer A. Rescaling the problem with the scalings in Figure 4, we find that the problem is defined by

$$(3.1a) \quad \frac{\partial \hat{c}_s}{\partial t} = \epsilon^2 \hat{D} \frac{\partial^2 \hat{c}_s}{\partial z^2}, \quad \frac{\partial T_s}{\partial t} = \kappa \frac{\partial^2 T_s}{\partial z^2} \quad \text{on } S(t) < z < 1,$$

$$(3.1b) \quad \frac{\partial \hat{c}_s}{\partial z} = 0 \quad \text{and} \quad T_s = -1 \quad \text{at } z = 1$$

and, as initially all the silicon is liquid (so $S(0) = 1$), we have no initial conditions. The problem is completed with the corresponding matching conditions with layer B, which are discussed in section 3.1.4. We expand \hat{c}_s , T_s , and S as $\hat{c}_s = \hat{c}_{s0} + \epsilon \hat{c}_{s1} + \mathcal{O}(\epsilon^2)$, $T_s = T_{s0} + \epsilon T_{s1} + \mathcal{O}(\epsilon^2)$, and $S = S_0 + \epsilon S_1 + \mathcal{O}(\epsilon^2)$.

At $\mathcal{O}(1)$, and using the matching conditions determined in section 3.1.4, the problem for the concentration field is

$$(3.2a) \quad \frac{\partial \hat{c}_{s0}}{\partial t} = 0,$$

$$(3.2b) \quad \hat{c}_{s0} = \hat{c}_i(t) \quad \text{at } z = S_0(t),$$

where $c_i(t)$ is the concentration at the interface which is yet to be determined. The problem for the temperature field is

$$(3.3a) \quad \frac{\partial T_{s0}}{\partial t} = \kappa \frac{\partial^2 T_{s0}}{\partial z^2},$$

$$(3.3b) \quad T_{s0} = 0 \quad \text{and} \quad \frac{\rho}{St} S'_0(t) = k \frac{\partial T_{s0}}{\partial z} \quad \text{at } z = S_0(t), \quad T_{s0} = -1 \quad \text{at } z = 1,$$

which is a classical one-phase Stefan problem. We find the solutions

$$(3.4) \quad \hat{c}_{s0} = \hat{\alpha}c_i(S_0^{-1}(z)), \quad T_{s0} = -1 + \frac{\operatorname{erf}\left(\frac{1-z}{2\sqrt{\kappa t}}\right)}{\operatorname{erf}\left(\frac{\lambda}{\sqrt{\kappa}}\right)} \quad \text{with} \quad S_0 = 1 - 2\lambda\sqrt{t},$$

where λ is a constant to be determined, as shown in section 3.1.4. Notice that the expression for \hat{c}_{s0} implies that the concentration in the solid at each point remains equal to the value it had at the moment it solidified, which is a fraction $\hat{\alpha}$ of the interfacial concentration in the liquid c_i .

At $\mathcal{O}(\epsilon)$, we consider only the temperature problem as the concentration is not required for the purpose of our analysis. Using the $\mathcal{O}(1)$ solutions, we have the problem

$$(3.5a) \quad \frac{\partial T_{s1}}{\partial t} = \kappa \frac{\partial^2 T_{s1}}{\partial z^2} \quad \text{in} \quad 1 - 2\lambda\sqrt{t} < z < 1,$$

$$(3.5b) \quad T_{s1} = -\frac{c_i}{\hat{m}_l} + \frac{\lambda}{k\sqrt{t}} \frac{\rho}{\text{St}} S_1(t) \quad \text{at} \quad z = 1 - 2\lambda\sqrt{t}, \quad \text{and} \quad T_{s1} = 0 \quad \text{at} \quad z = 1,$$

while the initial condition is not defined in this region.

We rescale the problem introducing the variable $\eta = \frac{z-S_0(t)}{1-S_0(t)}$, where $S_0(t) = 1 - 2\lambda\sqrt{t}$. This change of variable fixes the domain of the problem to $\eta \in [0, 1]$. The transformed problem reads

$$(3.6a) \quad 4\lambda^2 t \frac{\partial T_{s1}}{\partial t} = \kappa \frac{\partial^2 T_{s1}}{\partial \eta^2} - 2\lambda(1-\eta) \frac{\partial T_{s1}}{\partial \eta} \quad \text{in} \quad 0 < \eta < 1,$$

$$(3.6b) \quad T_{s1} = -\frac{c_i}{\hat{m}_l} + \frac{\lambda}{k\sqrt{t}} \frac{\rho}{\text{St}} S_1(t) \quad \text{at} \quad \eta = 0, \quad \text{and} \quad T_{s1} = 0 \quad \text{at} \quad \eta = 1.$$

This has no simple analytical solution so, in order to solve this problem, we shall assume $\lambda \ll 1$ and expand the solutions in powers of λ : $T_{s1} = T_{s1,0} + \lambda T_{s1,1} + \mathcal{O}(\lambda^2)$. As can be found from the transcendental equation (3.33), we have $\lambda \sim \sqrt{\text{St}}$ so this limit of small λ is equivalent to the small Stefan number limit. Hence, with the expansion for small λ here, we are taking the limit $\text{St} \rightarrow 0$ independently of the limit $\epsilon \rightarrow 0$, in which we have expanded our problem initially. The physical meaning of the limit $\epsilon \rightarrow 0$ is that mass diffusion happens at a much slower time scale than heat diffusion does. The limit $\text{St} \rightarrow 0$ means that the time scale of the motion of the interface is much smaller than the thermal diffusive time scale. We expect the concentration profile to be driven by the motion of the interface, which corresponds to the limit $\epsilon \ll \text{St} \ll 1$, which in terms of time scales means that the solute diffusion time scale is much smaller than the interface motion time scale, which in turn is much smaller than the heat diffusion time scale. Mathematically, this condition ensures that we can first take the small epsilon limit, and second the small Stefan number limit. In terms of λ , we require $\epsilon \ll \lambda^2 \ll 1$ so we can take the limits $\epsilon \rightarrow 0$ and $\lambda \rightarrow 0$ independently.

The leading order problem is

$$(3.7a) \quad \frac{\partial^2 T_{s1,0}}{\partial \eta^2} = 0 \quad \text{in} \quad 0 < \eta < 1,$$

$$(3.7b) \quad T_{s1,0} = -\frac{c_i}{\hat{m}_l} \quad \text{at} \quad \eta = 0, \quad \text{and} \quad T_{s1,0} = 0 \quad \text{at} \quad \eta = 1,$$

and we find that

$$(3.8) \quad T_{s1,0} = -\frac{c_i}{\hat{m}_l}(1-\eta).$$

At $\mathcal{O}(\lambda)$, the problem is

$$(3.9a) \quad \kappa \frac{\partial^2 T_{s1,1}}{\partial \eta^2} = 2(1-\eta) \frac{\partial T_{s1,0}}{\partial \eta} \quad \text{in } 0 < \eta < 1,$$

$$(3.9b) \quad T_{s1,1} = \frac{1}{k\sqrt{t}} \frac{\rho}{St} S_1(t) \quad \text{at } \eta = 0 \quad \text{and} \quad T_{s1,1} = 0 \quad \text{at } \eta = 1,$$

and we find

$$(3.10) \quad T_{s1,1} = (1-\eta) \left(-\frac{c_i}{\hat{m}_l} \frac{(2-\eta)\eta}{3\kappa} + \frac{\rho}{kSt} \frac{S_1(t)}{\sqrt{t}} \right).$$

We can proceed similarly to determine higher order solutions.

3.1.2. Layer B. Layer B is the inner layer of size ϵ around the moving interface. Therefore we define the inner variable $Z = \frac{z-S(t)}{\epsilon}$ and, using the other scalings defined in Figure 4, we find that the problem is

$$(3.11a) \quad \epsilon \frac{\partial \hat{c}_s}{\partial t} = S'(t) \frac{\partial \hat{c}_s}{\partial Z} + \epsilon \hat{D} \frac{\partial^2 \hat{c}_s}{\partial Z^2}, \quad \epsilon^2 \frac{\partial \hat{T}_s}{\partial t} = \epsilon S'(t) \frac{\partial \hat{T}_s}{\partial Z} + \kappa \frac{\partial^2 \hat{T}_s}{\partial Z^2} \quad \text{on } Z > 0,$$

$$(3.11b) \quad \epsilon \frac{\partial c_l}{\partial t} = S'(t) \frac{\partial c_l}{\partial Z} + \frac{\partial^2 c_l}{\partial Z^2}, \quad \epsilon^2 \frac{\partial \hat{T}_l}{\partial t} = \epsilon S'(t) \frac{\partial \hat{T}_l}{\partial Z} + \frac{\partial^2 \hat{T}_l}{\partial Z^2} \quad \text{on } Z < 0,$$

$$(3.11c) \quad \hat{T}_s = \hat{T}_l, \quad \hat{c}_s = \hat{\alpha} c_l, \quad c_l = -\hat{m}_l \hat{T}_l, \\ \frac{\rho}{St} \frac{dS}{dt} = k \frac{\partial \hat{T}_s}{\partial Z} - \frac{\partial \hat{T}_l}{\partial Z}, \quad (1 - \epsilon \hat{\alpha}) c_l \frac{dS}{dt} = \epsilon^2 \hat{D} \frac{\partial \hat{c}_s}{\partial Z} - \frac{\partial c_l}{\partial Z}$$

at the interface ($Z = 0$). The remaining conditions are given by the matching with the solutions in layers A and C. At $\mathcal{O}(1)$, (3.11) gives

$$(3.12a) \quad S'_0(t) \frac{\partial \hat{c}_{s0}}{\partial Z} = 0, \quad \frac{\partial^2 \hat{T}_{s0}}{\partial Z^2} = 0, \quad S'_0(t) \frac{\partial c_{l0}}{\partial Z} + \frac{\partial^2 c_{l0}}{\partial Z^2} = 0, \quad \frac{\partial^2 \hat{T}_{l0}}{\partial Z^2} = 0,$$

$$(3.12b) \quad \hat{T}_{s0} = \hat{T}_{l0}, \quad \hat{c}_{s0} = \hat{\alpha} c_{l0}, \quad c_{l0} = -\hat{m}_l \hat{T}_{l0}, \quad \frac{\rho}{St} \frac{dS_0}{dt} = k \frac{\partial \hat{T}_{s0}}{\partial Z} - \frac{\partial \hat{T}_{l0}}{\partial Z}, \quad c_{l0} \frac{dS_0}{dt} + \frac{\partial c_{l0}}{\partial Z} = 0$$

at the interface ($Z = 0$). Solving the system (3.12) with the matching conditions derived in section 3.1.4 we find

$$(3.13a) \quad \hat{c}_{s0} = \hat{\alpha} c_i(t), \quad \hat{T}_{s0} = A_1(t)Z - \frac{c_i(t)}{\hat{m}_l},$$

$$(3.13b) \quad c_{l0} = c_i(t)e^{-S'_0(t)Z}, \quad \hat{T}_{l0} = \left(kA_1(t) - \frac{\rho}{St} S'_0(t) \right) Z - \frac{c_i(t)}{\hat{m}_l},$$

where $c_i(t)$ is the concentration of the interface and $A_1(t)$ an integration function, both to be determined by the matching conditions.

Meanwhile, at $\mathcal{O}(\epsilon)$, (3.11) gives

$$(3.14a) \quad S'_0(t) \frac{\partial \hat{c}_{s1}}{\partial Z} = \frac{\partial \hat{c}_{s0}}{\partial t} - S'_1(t) \frac{\partial \hat{c}_{s0}}{\partial Z} - \hat{D} \frac{\partial^2 \hat{c}_{s0}}{\partial Z^2}, \quad \kappa \frac{\partial^2 \hat{T}_{s1}}{\partial Z^2} = -S'_0(t) \frac{\partial \hat{T}_{s0}}{\partial Z},$$

$$(3.14b) \quad S'_0(t) \frac{\partial c_{l1}}{\partial Z} + \frac{\partial^2 c_{l1}}{\partial Z^2} = \frac{\partial c_{l0}}{\partial t} - S'_1(t) \frac{\partial c_{l0}}{\partial Z}, \quad \frac{\partial^2 \hat{T}_{l1}}{\partial Z^2} = -S'_0(t) \frac{\partial \hat{T}_{l0}}{\partial Z},$$

$$(3.14c) \quad \hat{T}_{s1} = \hat{T}_{l1}, \quad \hat{c}_{s1} = \hat{a}c_{l1}, \quad c_{l1} = -\hat{m}_l \hat{T}_{l1}, \quad \frac{\rho}{St} \frac{dS_1}{dt} = k \frac{\partial \hat{T}_{s1}}{\partial Z} - \frac{\partial \hat{T}_{l1}}{\partial Z},$$

$$c_{l1} \frac{dS_0}{dt} + \frac{\partial c_{l1}}{\partial Z} = c_{l0} \left(\hat{a} \frac{dS_0}{dt} - \frac{dS_1}{dt} \right)$$

at the interface ($Z = 0$). The solutions to (3.14) are

$$(3.15a) \quad \hat{c}_{s1} = \frac{\hat{a}c'_i(t)}{S'_0(t)} Z + \hat{a}\mathcal{A}_2(t), \quad \hat{T}_{s1} = -\frac{A_1(t)S'_0(t)}{2\kappa} Z^2 + A_3(t)Z - \frac{\mathcal{A}_2(t)}{\hat{m}_l},$$

$$(3.15b) \quad c_{l1} = \mathcal{A}_1(t) + \mathcal{A}_3(t, Z)e^{-S'_0(t)Z},$$

$$\hat{T}_{l1} = -\frac{S'_0(t)}{2} \left(kA_1(t) - \frac{\rho}{St} S'_0(t) \right) Z^2 + \left(kA_3(t) - \frac{\rho}{St} S'_1(t) \right) Z - \frac{\mathcal{A}_2(t)}{\hat{m}_l}$$

with

$$(3.16a)$$

$$\mathcal{A}_1(t) = \frac{c'_i(t)}{S'_0(t)^2} + c_i(t) \left(\hat{a} - \frac{S''_0(t)}{S'_0(t)^3} \right), \quad \mathcal{A}_2(t) = A_2(t) + c_i(t) \left(\hat{a} - \frac{S'_1(t)}{S'_0(t)} \right),$$

$$(3.16b)$$

$$\mathcal{A}_3(t, Z) = -\frac{c'_i(t)}{S'_0(t)^2} (1 + S'_0(t)Z) + A_2(t)$$

$$- c_i(t) \left[\frac{S'_1(t)}{S'_0(t)} (1 + S'_0(t)Z) + \frac{S''_0(t)}{S'_0(t)^3} \left(1 + S'_0(t)Z + \frac{1}{2} S'_0(t)^2 Z^2 \right) \right],$$

where $A_2(t)$, and $A_3(t)$ are determined from asymptotic matching with other regions.

3.1.3. Layer C. The last layer in regime i is layer C, the outer layer in the liquid ($0 < z < S(t)$). Rescaling the problem according to Figure 4, we find that

$$(3.17a) \quad \frac{\partial \hat{c}_l}{\partial t} = \epsilon \frac{\partial^2 \hat{c}_l}{\partial z^2}, \quad \frac{\partial \hat{T}_l}{\partial t} = \frac{\partial^2 \hat{T}_l}{\partial z^2},$$

$$(3.17b)$$

$$\frac{\partial \hat{c}_l}{\partial z} = 0 \quad \text{and} \quad \frac{\partial \hat{T}_l}{\partial z} = 0 \quad \text{at} \quad z = 0, \quad \text{and} \quad \hat{c}_l = \hat{c}_0 \quad \text{and} \quad \hat{T}_l = \hat{T}_0 \quad \text{at} \quad t = 0,$$

and we can complete the problem with the matching conditions with layer B, which are discussed in section 3.1.4. At $\mathcal{O}(1)$, the problem is

$$(3.18a) \quad \frac{\partial \hat{c}_{l0}}{\partial t} = 0, \quad \frac{\partial \hat{T}_{l0}}{\partial t} = \frac{\partial^2 \hat{T}_{l0}}{\partial z^2},$$

$$(3.18b)$$

$$\frac{\partial \hat{T}_{l0}}{\partial z} = 0 \quad \text{at} \quad z = 0, \quad \hat{T}_{l0} = -\frac{c_i}{\hat{m}_l} \quad \text{at} \quad z = S_0(t), \quad \hat{c}_{l0} = \hat{c}_0, \quad \text{and} \quad \hat{T}_{l0} = \hat{T}_0 \quad \text{at} \quad t = 0.$$

We find $\hat{c}_{l0} = \hat{c}_0$. In order to determine \hat{T}_{l0} we introduce the variable $\xi = \frac{z}{S_0(t)}$, to fix the domain of the equation to $\xi \in [0, 1]$, and the rescaling for the temperature from \hat{T}_{l0} to u where

$$(3.19) \quad \hat{T}_{l0} = \left(\hat{T}_0 + \frac{c_i}{\hat{m}_l} \right) u - \frac{c_i}{\hat{m}_l},$$

to homogenize the boundary conditions. Then, the problem can be rewritten as

$$(3.20a) \quad \frac{\partial u}{\partial t} = \frac{1}{(1 - 2\lambda\sqrt{t})^2} \frac{\partial^2 u}{\partial \xi^2} - \xi \frac{\lambda}{\sqrt{t}(1 - 2\lambda\sqrt{t})} \frac{\partial u}{\partial \xi} \quad \text{in } 0 < \xi < 1,$$

$$(3.20b) \quad \frac{\partial u}{\partial \xi} = 0 \quad \text{at } \xi = 0, \quad u = 0 \quad \text{at } \xi = 1, \quad u = 1 \quad \text{when } t = 0.$$

Again no simple analytical solution is possible so, in order to solve the problem, we assume that $\lambda \ll 1$ and we expand u in powers of λ . The problem at $\mathcal{O}(1)$ is given by

$$(3.21a) \quad \frac{\partial u_0}{\partial t} = \frac{\partial^2 u_0}{\partial \xi^2} \quad \text{in } 0 < \xi < 1,$$

$$(3.21b) \quad \frac{\partial u_0}{\partial \xi} = 0 \quad \text{at } \xi = 0, \quad u_0 = 0 \quad \text{at } \xi = 1, \quad u_0 = 1 \quad \text{when } t = 0.$$

We use separation of variables to solve (3.21), obtaining

$$(3.22) \quad u_0 = \frac{4}{\pi} \sum_{n=0}^{\infty} \frac{(-1)^n}{2n+1} e^{-(\frac{2n+1}{2}\pi)^2 t} \cos\left(\frac{2n+1}{2}\pi\xi\right).$$

Higher order problems have the structure

$$(3.23a) \quad \frac{\partial u_j}{\partial t} - \frac{\partial^2 u_j}{\partial \xi^2} = f_j(t, \xi) \quad \text{in } 0 < \xi < 1,$$

$$(3.23b) \quad \frac{\partial u_j}{\partial \xi} = 0 \quad \text{at } \xi = 0, \quad u_j = 0 \quad \text{at } \xi = 1, \quad u_j = 0 \quad \text{when } t = 0$$

for $j > 1$. In all the cases, the function $f_j(t, \xi)$ is a known function that depends on the lower order solutions. We can find the solution to each problem using the Green's function $\mathcal{G}(\xi, \hat{\xi}, t - \tau)$ which gives

$$(3.24) \quad u_j(t, \xi) = \int_0^t \int_0^1 f_j(\tau, \hat{\xi}) \mathcal{G}(\xi, \hat{\xi}, t - \tau) d\hat{\xi} d\tau,$$

and from [29] we know that the Green's function for the problem can be represented in the two forms

$$(3.25) \quad \begin{aligned} \mathcal{G}(\xi, \hat{\xi}, t) &= 2 \sum_{n=0}^{\infty} \cos\left(\frac{2n+1}{2}\pi\xi\right) \cos\left(\frac{2n+1}{2}\pi\hat{\xi}\right) e^{-(\frac{2n+1}{2}\pi)^2 t} \\ &= \frac{1}{2\sqrt{\pi t}} \sum_{n=-\infty}^{n=+\infty} (-1)^n \left(e^{-\frac{(\xi-\hat{\xi}+2n)^2}{4t}} + e^{-\frac{(\xi+\hat{\xi}+2n)^2}{4t}} \right), \end{aligned}$$

where the first form converges rapidly at large t while the second form converges rapidly at small t .

3.1.4. Matching of the solutions. In this section we use Van Dyke’s rule [38] to derive the matching conditions we have used to complete the problems in the previous sections. The notation to denote the asymptotic expansions is the following. By $(mti)(nto)$ we mean taking n terms in the outer solution written in terms of the inner variable and expanded to m th order in the inner variable. Similarly, by $(nto)(mti)$ we mean taking m terms in the inner solution written in terms of the outer variable and expanded to n th order in the outer variable. Van Dyke’s rule states that these two expansions have to be equal for any n and m .

We start matching c_l between the outer layer C and the inner layer B. We take two terms in the inner solution and two terms in the outer solution and write them both in terms of the inner variable so $(2ti)(2to) = \epsilon \hat{c}_0$, $(2to)(2ti) = \epsilon \mathcal{A}_1(t)$, therefore we have

$$(3.26) \quad \frac{c'_i(t)}{S'_0(t)^2} + c_i(t) \left(\hat{\alpha} - \frac{S''_0(t)}{S'_0(t)^3} \right) = \hat{c}_0,$$

and solving this ODE for $c_i(t)$ using as initial condition that $c_i(t)$ must remain bounded we determine that c_i is constant and equal to $c_i = \frac{2\lambda^2 \hat{c}_0}{2\lambda^2 \hat{\alpha} + 1}$.

We then match c_s between the outer layer A and the inner layer B. We take two terms in the inner solution and two terms in the outer solution and write them both in terms of the inner variable so $(2ti)(2to) = \epsilon c_{s0}(S_0(t))$, $(2to)(2ti) = \epsilon \hat{\alpha} c_i(t)$, and equating both expressions, we find $c_{s0}(z) = \hat{\alpha} c_i$.

We repeat the procedure for T_s and T_l . For the simplicity of the calculations, we start expanding one term of the inner solution and one term of the outer in T_s to determine S_0 . Then, we find

$$(3.27) \quad (1ti)(1to) = -1 + C_1 \operatorname{erf} \left(\frac{1 - S_0(t)}{2\sqrt{\kappa t}} \right) = 0 = (1to)(1ti),$$

where C_1 is a constant yet to be determined, so we require the interface position to be of the form $S_0(t) = 1 - 2\lambda\sqrt{t}$, determining thus the result in (3.4). We can use this expression to simplify the following expansions. We now take three terms in the outer solution (the term at $\mathcal{O}(\epsilon^2)$ is left as $T_{s2}(t, z)$ for simplicity) and three terms in the inner solution which give

$$(3.28a) \quad \begin{aligned} (3ti)(3to) &= \left(-1 + C_1 \operatorname{erf} \left(\frac{\lambda}{\sqrt{\kappa}} \right) \right) + \epsilon \left(T_{s1}|_{z=S_0(t)} - C_1 e^{-\frac{\lambda^2}{\kappa}} \frac{Z + S_1(t)}{\sqrt{\pi \kappa t}} \right) \\ &+ \epsilon^2 \left(-\frac{e^{-\frac{\lambda^2}{\kappa}}}{2\sqrt{\pi t \kappa^{\frac{3}{2}}}} \left(C_1 \lambda (Z + S_1(t))^2 + 2C_1 \kappa \sqrt{t} S_2(t) \right) \right. \\ &\quad \left. + (Z + S_1(t)) \frac{\partial T_{s1}}{\partial z} \Big|_{z=S_0(t)} + T_{s2}|_{z=S_0(t)} \right), \end{aligned}$$

$$(3.28b) \quad (3to)(3ti) = \epsilon \left(A_1(t)Z - \frac{c_i}{\hat{m}_l} \right) + \epsilon^2 \left(-\frac{A_1(t)S'_0(t)}{2\kappa} Z^2 + A_3(t)Z - \frac{A_2(t)}{\hat{m}_l} \right),$$

and we determine that

$$(3.29a) \quad C_1 = \frac{1}{\operatorname{erf} \left(\frac{\lambda}{\sqrt{\kappa}} \right)},$$

$$(3.29b) \quad T_{s1}|_{z=S_0(t)} = \frac{\lambda}{\kappa \sqrt{t}} \frac{S_1(t)}{G \left(\frac{\lambda}{\sqrt{\kappa}} \right)} - \frac{c_i}{\hat{m}_l},$$

$$(3.29c) \quad A_1(t) = -\frac{\lambda}{\kappa\sqrt{t}} \frac{1}{G\left(\frac{\lambda}{\sqrt{\kappa}}\right)},$$

$$(3.29d) \quad A_3(t) = \frac{\partial T_{s1}}{\partial z} \Big|_{z=S_0(t)} - \frac{\lambda^2}{\kappa^2 t} \frac{S_1(t)}{G\left(\frac{\lambda}{\sqrt{\kappa}}\right)},$$

where $G(x) = \sqrt{\pi} x e^{x^2} \operatorname{erf}(x)$.

We proceed similarly for T_i . Taking three term inner and outer expansions, we find

(3.30a)

$$(3ti)(3to) = \epsilon \hat{T}_{i0}(t, S_0(t)) + \epsilon^2 \left((Z + S_1(t)) \frac{\partial \hat{T}_{i0}}{\partial z} \Big|_{z=S_0(t)} + \hat{T}_{i1}(t, S_0(t)) \right),$$

$$(3to)(3ti) = \epsilon \left[\left(kA_1(t) - \frac{\rho}{\operatorname{St}} S_0'(t) \right) Z - \frac{c_i}{\hat{m}_l} \right]$$

$$(3.30b) \quad + \epsilon^2 \left[-\frac{S_0'(t)}{2} \left(kA_1(t) - \frac{\rho}{\operatorname{St}} S_0'(t) \right) Z^2 + \left(kA_3(t) - \frac{\rho}{\operatorname{St}} S_1'(t) \right) Z - \frac{A_3(t)}{\hat{m}_l} \right],$$

and we determine that

$$(3.31a) \quad \hat{T}_{i0}(t, S_0(t)) = -\frac{c_i}{\hat{m}_l},$$

$$(3.31b) \quad kA_1(t) - \frac{\rho}{\operatorname{St}} S_0'(t) = 0,$$

$$(3.31c) \quad \frac{\partial \hat{T}_{i0}}{\partial z} \Big|_{z=S_0(t)} = kA_3(t) - \frac{\rho}{\operatorname{St}} S_1'(t).$$

We can use (3.31) to determine λ , S_1 , and the boundary conditions required to complete the \hat{T}_{i0} problem (3.20). We start by finding λ . We know that

$$(3.32) \quad \frac{\rho}{\operatorname{St}} S_0'(t) = kA_1(t),$$

and given that both $S_0(t)$ and $A_1(t)$ are known from (3.4) and (3.29c), we have

$$(3.33) \quad \sqrt{\pi} \frac{\lambda}{\sqrt{\kappa}} e^{\frac{\lambda^2}{\kappa}} \operatorname{erf}\left(\frac{\lambda}{\sqrt{\kappa}}\right) = c_p \operatorname{St},$$

and solving this transcendental equation we find λ . The condition (3.31a) determines the remaining boundary condition needed for the problem for \hat{T}_{i0} (3.20).

From condition (3.31c) and using (3.29d) we find

$$(3.34) \quad \frac{\rho}{\operatorname{St}} \left(S_1'(t) + \frac{\lambda^2}{\kappa t} S_1(t) \right) = k \frac{\partial \hat{T}_{s1}}{\partial z} \Big|_{z=S_0(t)} - \frac{\partial \hat{T}_{i0}}{\partial z} \Big|_{z=S_0(t)},$$

and integrating this equation we can determine $S_1(t)$. However, as we have the temperature gradients in terms of series in λ in (3.8) and (3.22), we can write

$$(3.35) \quad \frac{\rho}{\operatorname{St}} \left(S_1'(t) + \frac{\lambda^2}{\kappa t} S_1(t) \right) = \frac{k}{2\lambda\sqrt{t}} \left(\frac{c_i}{\hat{m}_l} + \mathcal{O}(\lambda) \right) + \frac{2}{1 - 2\lambda\sqrt{t}} \left(\hat{T}_0 + \frac{c_i}{\hat{m}_l} \right) \left(\sum_{n=0}^{\infty} e^{-(\frac{2n+1}{2}\pi)^2 t} + \mathcal{O}(\lambda) \right),$$

therefore we see that the temperature gradient in the solid is of $\mathcal{O}(\lambda^{-1})$ and hence $S_1(t)$ will also be this order. Expanding $S_1(t)$ in powers of λ , $S_1 = \lambda^{-1}S_{1,-1} + S_{1,0} + \mathcal{O}(\lambda)$, we have that, at $\mathcal{O}(\lambda^{-1})$, (3.35) is

$$(3.36) \quad \frac{\rho}{St} S'_{1,-1}(t) = \frac{k}{2\sqrt{t}} \frac{c_i}{\hat{m}_l},$$

therefore,

$$(3.37) \quad S_1(t) = \frac{kSt}{\rho} \frac{1}{2\lambda} \frac{c_i}{\hat{m}_l} \sqrt{t} + \mathcal{O}(1).$$

With this leading order approximation for $S_1(t)$ in powers of λ we conclude the analysis for regime i. This regime ranges for $t \in [0, t^*]$ where $t^* = \frac{1}{4\lambda^2}$ is the time when the leading order solution for the position of the interface becomes zero. In this regime, we have determined the solutions at leading order for all the variables and, for some of them, such as T_s , T_l , and S , we have determined the next term in the asymptotic expansion in powers of ϵ . The motivation to calculate these corrections was to determine the position of the interface up to $\mathcal{O}(\epsilon)$ as it is needed for the matching with the solution in regime ii. In the next section we focus our attention on regime ii, which arises because the interface is so close to the origin that the outer layer in the liquid disappears and, therefore, the inner layer needs to capture the symmetry conditions at the origin. Physically, this new regime captures the interaction between the two approaching solidification fronts caused by the diffusion of impurities in the liquid.

3.2. Asymptotic solutions in regime ii. We now study regime ii, where the interface is within a distance $\mathcal{O}(\epsilon)$ from the origin and therefore the mass diffusion boundary layer reaches the symmetry line. In this case we distinguish two layers: the outer layer D and the inner layer E.

3.2.1. Layer D. We consider first the outer layer D, using the rescalings defined in Figure 4. Then, the problem is defined on $0 < z < 1$ by

$$(3.38a) \quad \frac{\partial \hat{c}_s}{\partial \tau} = \epsilon^3 \hat{D} \frac{\partial^2 \hat{c}_s}{\partial z^2}, \quad \frac{\partial T_s}{\partial \tau} = \epsilon \kappa \frac{\partial^2 T_s}{\partial z^2},$$

$$(3.38b) \quad \frac{\partial \hat{c}_s}{\partial z} = 0 \quad \text{and} \quad T_s = -1 \quad \text{at} \quad z = 1,$$

and the appropriate matching conditions with layers A and E.

At $\mathcal{O}(1)$ the problem is

$$(3.39a) \quad \frac{\partial \hat{c}_{s0}}{\partial \tau} = 0, \quad \frac{\partial T_{s0}}{\partial \tau} = 0,$$

therefore, the leading order solutions do not depend on time, so we have to determine their values from matching with (3.4). We find

$$(3.40) \quad \hat{c}_{s0} = \frac{2\lambda^2 \hat{\alpha}}{2\lambda^2 \hat{\alpha} + 1} \hat{c}_0, \quad T_{s0} = -1 + \frac{\text{erf}\left(\frac{\lambda}{\sqrt{\kappa}}(1-z)\right)}{\text{erf}\left(\frac{\lambda}{\sqrt{\kappa}}\right)}.$$

3.2.2. Layer E. We determine the governing equations in the inner layer E using the scalings in Figure 4. The problem becomes

$$(3.41a) \quad \frac{\partial \hat{c}_s}{\partial \tau} = \epsilon \hat{D} \frac{\partial^2 \hat{c}_s}{\partial Z^2}, \quad \epsilon \frac{\partial \hat{T}_s}{\partial \tau} = \kappa \frac{\partial^2 \hat{T}_s}{\partial Z^2}, \quad \frac{\partial c_l}{\partial \tau} = \frac{\partial^2 c_l}{\partial Z^2}, \quad \epsilon \frac{\partial \hat{T}_l}{\partial \tau} = \frac{\partial^2 \hat{T}_l}{\partial Z^2},$$

$$(3.41b) \quad \hat{T}_s = \hat{T}_l, \quad \hat{c}_s = \hat{\alpha} c_l, \quad c_l = -\hat{m}_l \hat{T}_l, \quad \frac{\rho}{St} \frac{d\hat{S}}{d\tau} = k \frac{\partial \hat{T}_s}{\partial Z} - \frac{\partial \hat{T}_l}{\partial Z},$$

$$(1 - \epsilon \hat{\alpha}) c_l \frac{d\hat{S}}{d\tau} = \epsilon^2 \hat{D} \frac{\partial \hat{c}_s}{\partial Z} - \frac{\partial c_l}{\partial Z}$$

at the interface ($Z = \hat{S}(\tau)$),

$$(3.41c) \quad \frac{\partial c_l}{\partial Z} = 0 \quad \text{and} \quad \frac{\partial \hat{T}_l}{\partial Z} = 0 \quad \text{at } Z = 0.$$

We need to impose matching conditions in space with layer D and in time with layer B.

At $\mathcal{O}(1)$, we have

$$(3.42a) \quad \frac{\partial \hat{c}_{s0}}{\partial \tau} = 0, \quad \frac{\partial^2 \hat{T}_{s0}}{\partial Z^2} = 0, \quad \frac{\partial c_{l0}}{\partial \tau} = \frac{\partial^2 c_{l0}}{\partial Z^2}, \quad \frac{\partial^2 \hat{T}_{l0}}{\partial Z^2} = 0,$$

$$(3.42b) \quad \hat{T}_{s0} = \hat{T}_{l0}, \quad \hat{c}_{s0} = \hat{\alpha} c_{l0}, \quad c_{l0} = -\hat{m}_l \hat{T}_{l0},$$

$$\frac{\rho}{St} \frac{d\hat{S}_0}{d\tau} = k \frac{\partial \hat{T}_{s0}}{\partial Z} - \frac{\partial \hat{T}_{l0}}{\partial Z}, \quad c_{l0} \frac{d\hat{S}_0}{d\tau} + \frac{\partial c_{l0}}{\partial Z} = 0$$

at the interface ($Z = \hat{S}_0(\tau)$),

$$(3.42c) \quad \frac{\partial c_{l0}}{\partial Z} = 0 \quad \text{and} \quad \frac{\partial \hat{T}_{l0}}{\partial Z} = 0 \quad \text{at } Z = 0.$$

We obtain the leading order solutions

$$(3.43a) \quad \hat{c}_{s0} = \hat{\alpha} c_{l0} \left(\hat{S}_0^{-1}(Z), Z \right), \quad c_{l0} = c_{l0}(\tau, Z),$$

(3.43b)

$$\hat{T}_{s0} = \frac{\rho}{kSt} \frac{d\hat{S}_0}{d\tau} Z - \left(\frac{\rho}{kSt} \frac{d\hat{S}_0}{d\tau} \hat{S}_0(\tau) + \frac{c_{l0}(\tau, \hat{S}_0(\tau))}{\hat{m}_l} \right), \quad \hat{T}_{l0} = -\frac{c_{l0}(\tau, \hat{S}_0(\tau))}{\hat{m}_l},$$

where the function c_{l0} is yet to be determined. The problem for c_{l0} is given by

$$(3.44a) \quad \frac{\partial c_{l0}}{\partial \tau} = \frac{\partial^2 c_{l0}}{\partial Z^2},$$

$$(3.44b) \quad \frac{\partial c_{l0}}{\partial Z} = 0 \quad \text{at } Z = 0, \quad c_{l0} \frac{\partial \hat{S}_0}{\partial \tau} + \frac{\partial c_{l0}}{\partial Z} = 0 \quad \text{at } Z = \hat{S}_0(\tau),$$

$$c_{l0} \sim c_i e^{2\lambda^2(Z+2\lambda^2(\tau-\tau^*))} \quad \text{as } \tau \rightarrow -\infty,$$

where

$$(3.45) \quad \hat{S}_0(\tau) = -2\lambda^2(\tau - \tau^*), \quad \tau^* = \frac{kSt}{\rho} \frac{1}{8\lambda^4} \frac{c_i}{\hat{m}_l}.$$

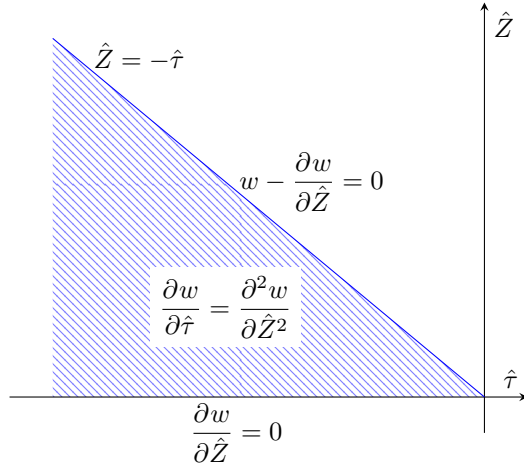


FIG. 5. Sketch of the problem (3.46). The highlighted area is the domain in which we want to solve the problem (which extends to $\hat{\tau} \rightarrow -\infty$). Then, we need to prescribe the initial condition when $\hat{\tau} \rightarrow -\infty$, which is $w \sim e^{\hat{Z}+\hat{\tau}}$.

We can eliminate all the parameters in the problem by rescaling the variables of the problem as $\tau = \frac{\hat{\tau}}{(2\lambda^2)^2} + \tau^*$, $Z = \frac{\hat{Z}}{2\lambda^2}$, $c_{i0} = c_i w$, and the problem reduces (as shown in Figure 5) to

$$(3.46a) \quad \frac{\partial w}{\partial \hat{\tau}} = \frac{\partial^2 w}{\partial \hat{Z}^2},$$

$$(3.46b) \quad \frac{\partial w}{\partial \hat{Z}} = 0 \quad \text{at} \quad \hat{Z} = 0, \quad w - \frac{\partial w}{\partial \hat{Z}} = 0 \quad \text{at} \quad \hat{Z} = -\hat{\tau}, \quad w \sim e^{\hat{Z}+\hat{\tau}} \quad \text{as} \quad \hat{\tau} \rightarrow -\infty.$$

We use the method of images to solve (3.46), finding

$$(3.47) \quad w(\hat{\tau}, \hat{Z}) = \sum_{n=1}^{\infty} n \left(e^{n(\hat{Z}+n\hat{\tau})} + e^{n(-\hat{Z}+n\hat{\tau})} \right).$$

It is immediate to check that (3.47) solves (3.46a) and the first condition in (3.46b) as each of the terms of the sum satisfies the equations. Truncating (3.47) at N terms, the error at the second condition in (3.46b) is $N(N+1)e^{N(N+1)\hat{\tau}}$ and given that $\hat{\tau} < 0$, it tends to zero as $N \rightarrow +\infty$. The exception is in the limit $\hat{\tau} \rightarrow 0^-$, however, this latter limit is considered separately in regime iii, which takes over before the singularity is reached, hence the solution (3.47) is valid for our purposes. Finally, it can be checked that (3.47) satisfies the initial condition in (3.46b).

3.2.3. Matching of the solutions. We start matching c_s between the outer layer in time B and the inner layer in time B. Taking two terms both in the inner and outer solution we find that the solution is constant so $c_s = \epsilon \hat{a} c_i$. In order to determine the initial conditions for c_l we need to match it with layer E. Taking one term in each solution we find

$$(3.48) \quad (1to)(1ti) = \lim_{\tau \rightarrow -\infty} c_{i0}(\tau, Z) = c_i \exp \left[2\lambda^2 \left(Z + 2\lambda^2 \left(\tau - \frac{kSt}{\rho} \frac{1}{8\lambda^4} \frac{c_i}{\hat{m}_l} \right) \right) \right] = (1ti)(1to).$$

Finally, we need to match T_s with layer D in order to determine the interface position $\hat{S}_0(\tau)$. Taking one term of the outer solution and two terms in the inner solution we find

$$(3.49) \quad (2ti)(1to) = -\epsilon \frac{\rho}{kSt} 2\lambda^2 Z, \quad (1to)(2ti) = \epsilon \frac{\rho}{kSt} \frac{d\hat{S}_0}{d\tau} Z;$$

therefore, we find $\hat{S}_0(\tau) = -2\lambda^2\tau + C_3$, and we need to determine C_3 from matching with regime i. Taking two terms in both the inner and outer solutions we find

$$(3.50) \quad (2ti)(2to) = \epsilon \left(-2\lambda^2\tau - \frac{kSt}{\rho} \frac{1}{4\lambda^2} \left(1 - \frac{c_i}{\hat{m}_l} \right) \right), \quad (2to)(2ti) = \epsilon (-2\lambda^2\tau + C_3),$$

hence

$$(3.51) \quad C_3 = -\frac{kSt}{\rho} \frac{1}{4\lambda^2} \left(1 - \frac{c_i}{\hat{m}_l} \right).$$

Thus, we have that the interface is linear and can reduce the problem for c_{l0} into (3.46).

We have now fully determined the leading order solutions in regime ii, which are mainly driven by the buildup of impurities in the liquid phase due to the fact that the two solidification fronts are very close to each other and therefore impurities cannot diffuse away. Because the concentration of impurities is small, compared to the amount required to cause significant supercooling, the limiting behavior when $\tau \rightarrow \tau^*$ results in an infinite amount of impurity concentration in an infinitely small region of liquid. This motivates the study of regime iii, in which we expect the buildup of impurities to continue, but now with an impact over the thermal problem, that in turn slows down the interface.

3.3. Asymptotic solutions in regime iii. We now focus on regime iii, which has three layers: the outer layer F, the intermediate layer G, and the inner layer H. In this regime, the buildup of impurities is so high that it causes enough supercooling to slow down the interface at lowest order.

3.3.1. Layer F. We consider first the outer layer F, with the rescalings shown in Figure 4. The problem on $0 < z < 1$ is given by

$$(3.52a) \quad \frac{\partial \hat{c}_s}{\partial \theta} = \epsilon^{\frac{10}{3}} \hat{D} \frac{\partial^2 \hat{c}_s}{\partial z^2}, \quad \frac{\partial T_s}{\partial \theta} = \epsilon^{\frac{4}{3}} \kappa \frac{\partial^2 T_s}{\partial z^2},$$

$$(3.52b) \quad \frac{\partial \hat{c}_s}{\partial z} = 0 \quad \text{and} \quad T_s = -1 \quad \text{at} \quad z = 1,$$

and the appropriate matching conditions with layers D and G. At leading order we find

$$(3.53) \quad \hat{c}_{s0} = \epsilon \frac{2\lambda^2 \hat{\alpha}}{2\lambda^2 \hat{\alpha} + 1} \hat{c}_0, \quad T_{s0} = -1 + \frac{\operatorname{erf}\left(\frac{\lambda}{\sqrt{\kappa}}(1-z)\right)}{\operatorname{erf}\left(\frac{\lambda}{\sqrt{\kappa}}\right)},$$

which are the same solutions as (3.40) in layer D.

3.3.2. Layer G. The next layer to study is the intermediate layer G, which is the layer where significant heat diffusion takes place. In this layer, defined by $\xi > 0$, we have

$$(3.54) \quad \frac{\partial \hat{c}_s}{\partial \theta} = \epsilon^2 \hat{D} \frac{\partial^2 \hat{c}_s}{\partial \xi^2}, \quad \frac{\partial \hat{T}_s}{\partial \theta} = \kappa \frac{\partial^2 \hat{T}_s}{\partial \xi^2},$$

with matching conditions with layers D, F, and H. At $\mathcal{O}(1)$ the problem is

$$(3.55) \quad \frac{\partial \hat{c}_{s0}}{\partial \theta} = 0, \quad \frac{\partial \hat{T}_{s0}}{\partial \theta} = \kappa \frac{\partial^2 \hat{T}_{s0}}{\partial \xi^2},$$

from where we immediately determine that $c_s = \epsilon \hat{c}_i$, where $c_i = \frac{2\lambda^2 \hat{c}_0}{2\lambda^2 \hat{\alpha} + 1}$. In order to determine \hat{T}_{s0} we need to find the boundary conditions of the problem from matching. Using the conditions derived in section 3.3.4 we can write the problem for \hat{T}_{s0} and \hat{S}_0 as

$$(3.56a) \quad \frac{\partial \hat{T}_{s0}}{\partial \theta} = \kappa \frac{\partial^2 \hat{T}_{s0}}{\partial \xi^2} \quad \text{in } \xi > 0,$$

$$(3.56b) \quad \hat{T}_{s0} = -\frac{c_{tot}}{\hat{m}_l} \frac{1}{\hat{S}_0(\theta)} \quad \text{at } \xi = 0, \quad \frac{\partial \hat{T}_{s0}}{\partial \xi} = \frac{\rho}{kSt} \hat{S}'_0(\theta) \quad \text{at } \xi = 0,$$

$$(3.56c) \quad \hat{T}_{s0} \sim -2\lambda^2 \frac{\rho}{kSt} \xi \quad \text{as } \xi \rightarrow +\infty, \theta \rightarrow -\infty, \quad \hat{S}'_0(\theta) \rightarrow -2\lambda^2 \quad \text{as } \theta \rightarrow -\infty.$$

By introducing the scaled variables

$$\begin{aligned} \hat{T}_{s0} &= \left(2 \frac{\kappa \lambda^2 \rho^2 c_{tot}}{k^2 \hat{m}_l St^2} \right)^{\frac{1}{3}} (u - x), & \hat{S}_0 &= \left(\frac{k^2 St^2 c_{tot}^2}{2\kappa \lambda^2 \hat{m}_l^2 \rho^2} \right)^{\frac{1}{3}} S, \\ \theta &= \left(\frac{k^2 St^2 c_{tot}^2}{16\kappa \lambda^8 \hat{m}_l^2 \rho^2} \right)^{\frac{1}{3}} t, & \xi &= \left(\frac{\kappa k St c_{tot}}{4\lambda^4 \hat{m}_l \rho} \right)^{\frac{1}{3}} x, \end{aligned}$$

we reduce the problem (3.56) to

$$(3.57a) \quad \frac{\partial u}{\partial t} = \frac{\partial^2 u}{\partial x^2} \quad \text{in } x > 0,$$

$$(3.57b) \quad u = -\frac{1}{S(t)} \quad \text{at } x = 0,$$

$$(3.57c) \quad \frac{\partial u}{\partial x} = \frac{dS}{dt} + 1 \quad \text{at } x = 0,$$

$$(3.57d) \quad \frac{\partial u}{\partial x} \rightarrow 0 \quad \text{at } x \rightarrow +\infty,$$

$$(3.57e) \quad u \rightarrow 0 \quad \text{when } t \rightarrow -\infty,$$

$$(3.57f) \quad \frac{dS}{dt} \rightarrow -1 \quad \text{when } t \rightarrow -\infty.$$

We can use (3.57a), (3.57b), (3.57d), and (3.57e) to determine the solution $u(t, x)$ using Laplace transforms. Notice that our problem starts at $t \rightarrow -\infty$, therefore, when taking the transform, we need to start at $t = -t_0$ and then take $t_0 \rightarrow \infty$. We find that the Laplace transform of $u(t, x)$, defined as $\bar{u}(p, x) = \mathcal{L}\{u\}(p)$, where p is the frequency variable, is

$$(3.58) \quad \bar{u}(p, x) = p \mathcal{L} \left\{ -\frac{1}{S(t)} \right\} (p) \frac{e^{-x\sqrt{p}}}{p}.$$

We can now take the inverse Laplace transform to obtain $u(t, x)$, which is given by

$$(3.59) \quad u(t, x) = \left(\frac{d}{dt} \left(-\frac{1}{S(t)} \right) \right) * \operatorname{erfc} \left(\frac{x}{2\sqrt{t}} \right),$$

where $*$ denotes the convolution defined as

$$(3.60) \quad F(t) * G(t) = \int_{-\infty}^t F(\tau)G(t - \tau) d\tau.$$

Therefore, $u(t, x)$ is given by

$$(3.61) \quad u(t, x) = \int_{-\infty}^t \frac{d}{dt} \left(-\frac{1}{S(\tau)} \right) \operatorname{erfc} \left(\frac{x}{2\sqrt{t - \tau}} \right) d\tau.$$

From here, we shall obtain the equation governing $S(t)$. We start by taking the derivative of (3.58) with respect to x , to find

$$(3.62) \quad \frac{\partial \bar{u}}{\partial x} = -p\mathcal{L} \left\{ -\frac{1}{S(t)} \right\} (p) \frac{e^{-x\sqrt{p}}}{\sqrt{p}},$$

so taking the inverse Laplace transform we obtain

$$(3.63) \quad \frac{\partial u}{\partial x} = - \left(\frac{d}{dt} \left(-\frac{1}{S(t)} \right) \right) * \left(\frac{e^{-\frac{x^2}{4t}}}{\sqrt{\pi t}} \right).$$

Evaluating (3.63) at $x = 0$, we have

$$(3.64) \quad \frac{\partial u}{\partial x} \Big|_{x=0} = -\frac{1}{\sqrt{\pi}} \int_{-\infty}^t \frac{S'(\tau)}{S(\tau)^2} \frac{d\tau}{\sqrt{t - \tau}},$$

and using the boundary condition (3.57c) we obtain the nonlinear integro-differential equation

$$(3.65) \quad \frac{dS}{dt} + 1 = -\frac{1}{\sqrt{\pi}} \int_{-\infty}^t \frac{S'(\tau)}{S(\tau)^2} \frac{d\tau}{\sqrt{t - \tau}},$$

which determines $S(t)$.

We cannot find an exact solution for $S(t)$, but, given that the problem (3.57) has no parameters, we can solve it numerically and then rescale the results for our original problem (3.56). In order to solve (3.57) we use a finite volume scheme. We start the simulation at $t = -100$ with $S = 100$ and $u = 0$, so they are consistent with the initial conditions. The simulation domain is taken to be $x \in [0, 1000]$ which simulations show to be large enough so the boundary at $x = 1000$ does not interfere significantly with the diffusion process. Figure 6 shows the numerical solution.

Even though we cannot find exact solutions to (3.65), we can determine the large time behavior of the solution. Notice that, in the limit $t \rightarrow -\infty$, the behavior is given by the initial condition $\frac{dS}{dt} \rightarrow -1$, hence, we have that $S \sim -(t - C_4)$, where C_4 is an integration constant. Because the problem (3.57) is invariant under time shifts, C_4 remains undetermined unless further matching conditions are derived.

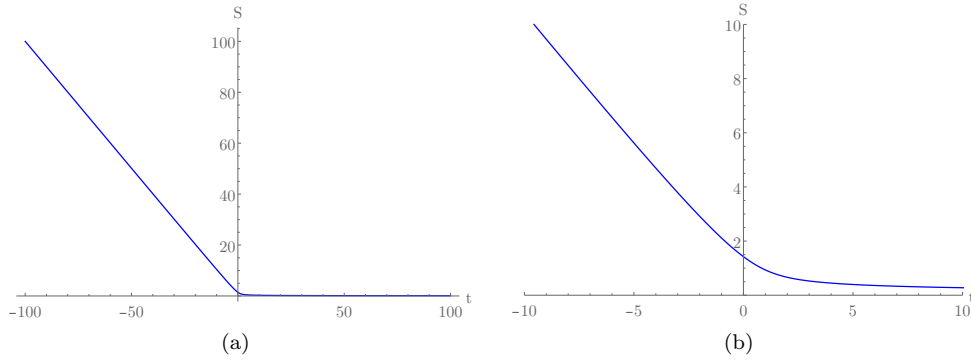


FIG. 6. Numerical solutions for $S(t)$ using (3.57) for (a) the range $t \in [-100, 100]$ and (b) the range $t \in [-10, 10]$.

The behavior in the limit $t \rightarrow +\infty$ can be found from (3.65), using the assumption that $\frac{dS}{dt} \rightarrow 0$ when $t \rightarrow +\infty$, which we have from the numerical solution. Then, (3.65) gives

$$(3.66) \quad 1 = -\frac{1}{\sqrt{\pi}} \int_{-\infty}^t \frac{S'(\tau)}{S(\tau)^2} \frac{d\tau}{\sqrt{t-\tau}} = -\frac{1}{\sqrt{\pi}} \left(\frac{S'(t)}{S(t)^2} \right) * \left(\frac{1}{\sqrt{t}} \right).$$

Taking the Laplace transform, we find

$$(3.67) \quad \frac{1}{p} = -\mathcal{L} \left\{ \frac{S'(t)}{S(t)^2} \right\} (p) \frac{1}{\sqrt{p}},$$

therefore,

$$(3.68) \quad \frac{1}{\sqrt{p}} = -\mathcal{L} \left\{ \frac{S'(t)}{S(t)^2} \right\} (p),$$

and taking the inverse Laplace transform we have

$$(3.69) \quad -\frac{S'(t)}{S(t)^2} = \frac{1}{\sqrt{\pi t}}.$$

Integrating, we conclude that

$$(3.70) \quad S(t) = \frac{\sqrt{\pi}}{2\sqrt{t} + C_5},$$

where C_5 is an integration constant. However, notice that when $t \rightarrow +\infty$, $S \sim \frac{\sqrt{\pi}}{2\sqrt{t}}$, therefore the value of this constant does not affect the asymptotic behavior of $S(t)$. Notice that this result satisfies the assumption $\frac{dS}{dt} \rightarrow 0$ when $t \rightarrow +\infty$ that we took at the beginning of the analysis. In Figure 7 we compare the behavior of the numerical simulations in both limits $t \rightarrow \pm\infty$ against the predictions on a loglog plot, finding that the numerical solutions agree with the expected asymptotic behavior.

3.3.3. Layer H. Finally, we study the inner layer H introducing the scalings described in Figure 4, where the interface conditions hold. The problem is

$$(3.71a) \quad \frac{\partial \hat{c}_s}{\partial \theta} = \epsilon^{\frac{2}{3}} \hat{D} \frac{\partial^2 \hat{c}_s}{\partial Z^2}, \quad \epsilon^{\frac{4}{3}} \frac{\partial \hat{T}_s}{\partial \theta} = \kappa \frac{\partial^2 \hat{T}_s}{\partial Z^2}, \quad \epsilon^{\frac{1}{3}} \frac{\partial \hat{c}_l}{\partial \theta} = \frac{\partial^2 \hat{c}_l}{\partial Z^2}, \quad \epsilon^{\frac{4}{3}} \frac{\partial \hat{T}_l}{\partial \theta} = \frac{\partial^2 \hat{T}_l}{\partial Z^2},$$

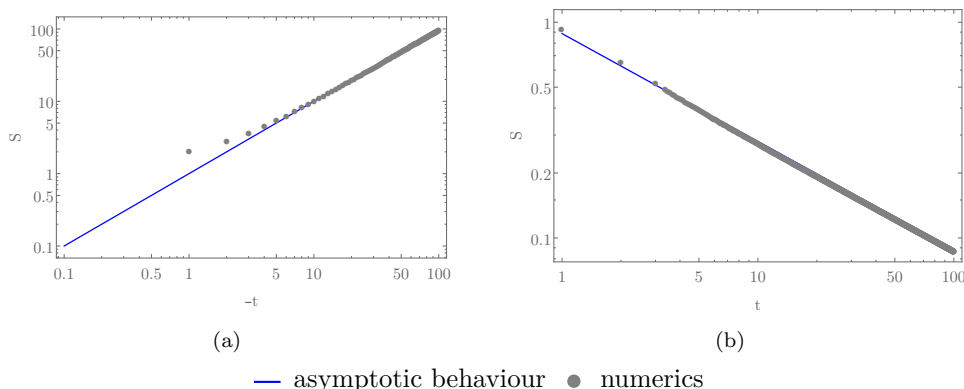


FIG. 7. Comparison of the numerical solutions and the asymptotic behavior of the solution to (3.65) in the limits (a) $t \rightarrow -\infty$ where the expected behavior is $S \sim -t$ given that for the initial conditions used in the simulations we have $C_4 = 0$ (notice that S is plotted against $-t$), and (b) $t \rightarrow +\infty$ where the expected behavior is $S \sim \frac{\sqrt{\pi}}{2\sqrt{t}}$.

$$(3.71b) \quad \hat{T}_s = \hat{T}_l, \quad \hat{c}_s = \hat{\alpha}\hat{c}_l, \quad \hat{c}_l = -\hat{m}_l\hat{T}_l,$$

$$\epsilon^{\frac{2}{3}} \frac{\rho}{St} \frac{d\hat{S}}{d\theta} = k \frac{\partial \hat{T}_s}{\partial Z} - \frac{\partial \hat{T}_l}{\partial Z}, \quad \epsilon^{\frac{1}{3}} (1 - \epsilon\hat{\alpha}) \hat{c}_l \frac{d\hat{S}}{d\theta} = \epsilon^2 \hat{D} \frac{\partial \hat{c}_s}{\partial Z} - \frac{\partial \hat{c}_l}{\partial Z}$$

at the interface ($Z = \hat{S}(\theta)$), and

$$(3.71c) \quad \frac{\partial \hat{c}_l}{\partial Z} = 0 \quad \text{and} \quad \frac{\partial \hat{T}_l}{\partial Z} = 0 \quad \text{at } Z = 0.$$

We need to impose appropriate matching conditions in space with layer G and in time with layer E.

The problem at $\mathcal{O}(1)$ is

$$(3.72a) \quad \frac{\partial \hat{c}_{s0}}{\partial \theta} = 0, \quad \frac{\partial^2 \hat{T}_{s0}}{\partial Z^2} = 0, \quad \frac{\partial^2 \hat{c}_{l0}}{\partial Z^2} = 0, \quad \frac{\partial^2 \hat{T}_{l0}}{\partial Z^2} = 0,$$

$$(3.72b) \quad \hat{T}_{s0} = \hat{T}_{l0}, \quad \hat{c}_{s0} = \hat{\alpha}\hat{c}_{l0}, \quad \hat{c}_{l0} = -\hat{m}_l\hat{T}_{l0}, \quad k \frac{\partial \hat{T}_{s0}}{\partial Z} = \frac{\partial \hat{T}_{l0}}{\partial Z}, \quad \frac{\partial \hat{c}_{l0}}{\partial Z} = 0$$

at the interface, and

$$(3.72c) \quad \frac{\partial \hat{c}_{l0}}{\partial Z} = 0 \quad \text{and} \quad \frac{\partial \hat{T}_{l0}}{\partial Z} = 0 \quad \text{at } Z = 0.$$

We find the solutions

$$(3.73) \quad \hat{c}_{s0} = \hat{\alpha}c_{i0}(\hat{S}_0^{-1}(Z)), \quad \hat{c}_{l0} = c_{i0}(\theta), \quad \hat{T}_{s0} = -\frac{c_{i0}(\theta)}{\hat{m}_l}, \quad \hat{T}_{l0} = -\frac{c_{i0}(\theta)}{\hat{m}_l},$$

where $c_{i0}(\theta)$ is the concentration at the interface, yet to be determined.

At $\mathcal{O}(\epsilon^{\frac{1}{3}})$, the problem is

$$(3.74a) \quad \frac{\partial \hat{c}_{s\frac{1}{3}}}{\partial \theta} = 0, \quad \frac{\partial^2 \hat{T}_{s\frac{1}{3}}}{\partial Z^2} = 0, \quad \frac{\partial^2 \hat{c}_{l\frac{1}{3}}}{\partial Z^2} = c'_{i0}(\theta), \quad \frac{\partial^2 \hat{T}_{l\frac{1}{3}}}{\partial Z^2} = 0,$$

$$(3.74b) \quad \hat{T}_{s\frac{1}{3}} = \hat{T}_{l\frac{1}{3}}, \quad \hat{c}_{s\frac{1}{3}} = \hat{\alpha} \left(\hat{c}_{l\frac{1}{3}} - \frac{\hat{S}_0(\theta)}{\hat{S}'_0(\theta)} c'_{i0}(\theta) \right), \quad \hat{c}_{l\frac{1}{3}} = -\hat{m}_l \hat{T}_{l\frac{1}{3}},$$

$$k \frac{\partial \hat{T}_{s\frac{1}{3}}}{\partial Z} = \frac{\partial \hat{T}_{l\frac{1}{3}}}{\partial Z}, \quad \frac{\partial \hat{c}_{l\frac{1}{3}}}{\partial Z} + c_{i0}(\theta) \frac{d\hat{S}_0}{d\theta} = 0$$

at the interface, and

$$(3.74c) \quad \frac{\partial \hat{c}_{l\frac{1}{3}}}{\partial Z} = 0 \quad \text{and} \quad \frac{\partial \hat{T}_{l\frac{1}{3}}}{\partial Z} = 0 \quad \text{at } Z = 0.$$

We obtain the solutions

$$(3.75) \quad \hat{c}_{l\frac{1}{3}} = \frac{1}{2} c'_{i0}(\theta) Z^2 + c_{i\frac{1}{3}}(\theta) - \frac{1}{2} c'_{i0}(\theta) \hat{S}_0(\theta)^2, \quad \hat{T}_{s\frac{1}{3}} = -\frac{c_{i\frac{1}{3}}(\theta)}{\hat{m}_l}, \quad \hat{T}_{l\frac{1}{3}} = -\frac{c_{i\frac{1}{3}}(\theta)}{\hat{m}_l},$$

and we do not calculate $c_{s\frac{1}{3}}$, since it is not useful to our analysis. We also find

$$(3.76) \quad \frac{\partial c_{i0}}{\partial \theta} \hat{S}_0 + c_{i0} \frac{\partial \hat{S}_0}{\partial \theta} = 0,$$

therefore, we conclude that $c_{i0} \hat{S}_0 = c_{tot}$ is constant. Note that this condition is equivalent to conservation of mass in the liquid at leading order, therefore, the constant c_{tot} is the total concentration of the problem in this regime. Furthermore, we can show that in regime ii the amount of impurities in the liquid at leading order is conserved, even though it is not constant. Therefore, the value of c_{tot} is constant throughout regimes ii and iii, so we can calculate it at the final state of regime i for convenience, that is using solution (3.13b). We find

$$(3.77) \quad c_{tot} = \int_{-\infty}^0 c_i e^{2\lambda^2 Z} dZ = \frac{\hat{c}_0}{2\lambda^2 \hat{\alpha} + 1}.$$

Finally, we study the problem at $\mathcal{O}(\epsilon^{\frac{2}{3}})$, however, we consider only the temperature profiles as they are the ones we need for the matching. We have

$$(3.78a) \quad \frac{\partial^2 \hat{T}_{s\frac{2}{3}}}{\partial Z^2} = 0 \quad \text{in } Z > \hat{S}_0(\theta), \quad \frac{\partial^2 \hat{T}_{l\frac{2}{3}}}{\partial Z^2} = 0 \quad \text{in } 0 < Z < \hat{S}_0(\theta),$$

$$(3.78b) \quad \frac{\rho}{St} \frac{d\hat{S}_0}{d\theta} = k \frac{\partial \hat{T}_{s\frac{2}{3}}}{\partial Z} - \frac{\partial \hat{T}_{l\frac{2}{3}}}{\partial Z} \quad \text{at } Z = \hat{S}_0(\theta), \quad \frac{\partial \hat{T}_{l\frac{2}{3}}}{\partial Z} = 0 \quad \text{at } Z = 0,$$

and we find the solutions

$$(3.79) \quad \hat{T}_{s\frac{2}{3}} = \frac{\rho}{kSt} \frac{d\hat{S}_0}{d\theta} Z + A_4(\theta), \quad \hat{T}_{l\frac{2}{3}} = A_4(\theta),$$

where $A_4(\theta)$ is related to the value of $c_{l\frac{2}{3}}$, which we have not calculated.

3.3.4. Matching of the solutions. We now match the solutions of the different layers to determine the boundary conditions for the temperature problem in layer G. We start by matching layers F and G; therefore, now G acts as the inner layer because F is the outer layer. Because in this regime we have the expansions of the solutions in powers of $\epsilon^{\frac{1}{3}}$, when we say we take two terms it means up to $\mathcal{O}(\epsilon^{\frac{1}{3}})$, three terms

means up to $\mathcal{O}(\epsilon^{\frac{2}{3}})$, and so on. Taking three terms in the inner solution and one term in the outer solution, we find

$$(3.80) \quad (3\text{ti})(1\text{to}) = \epsilon^{\frac{2}{3}} \left(-2\lambda^2 \frac{\rho}{k\text{St}} \xi \right), \quad (1\text{to})(3\text{ti}) = \lim_{\xi \rightarrow +\infty} \epsilon^{\frac{2}{3}} \hat{T}_{s0}(\theta, \xi),$$

therefore, we find the condition

$$(3.81) \quad \lim_{\xi \rightarrow +\infty} \hat{T}_{s0}(\theta, \xi) = -2\lambda^2 \frac{\rho}{k\text{St}} \xi.$$

Similarly, we determine the initial condition by matching the solution in layer G with the one in layer D. As the solution in layer D does not depend on time, we end up having the same linearization as in (3.81), therefore, we find

$$(3.82) \quad \lim_{\theta \rightarrow -\infty} \hat{T}_{s0}(\theta, \xi) = -2\lambda^2 \frac{\rho}{k\text{St}} \xi.$$

To complete the problem we need to calculate the matching between layer G and layer H, where now layer G acts as the outer layer. We take five terms in both layers finding

$$(3.83\text{a}) \quad (5\text{ti})(5\text{to}) = \epsilon^{\frac{2}{3}} \hat{T}_{s0}(\theta, 0) + \epsilon \hat{T}_{s\frac{1}{3}}(\theta, 0) + \epsilon^{\frac{4}{3}} \left(\frac{\partial \hat{T}_{s0}}{\partial Z} \Big|_{\xi=0} Z + \hat{T}_{s\frac{2}{3}}(\theta, 0) \right),$$

$$(3.83\text{b}) \quad (5\text{to})(5\text{ti}) = -\epsilon^{\frac{2}{3}} \frac{c_{i0}(\theta)}{\hat{m}_l} - \epsilon \frac{c_{i1}(\theta)}{\hat{m}_l} + \epsilon^{\frac{4}{3}} \left(\frac{\rho}{k\text{St}} \hat{S}'_0(\theta) Z + A_4(\theta) \right).$$

As we are only interested in determining \hat{T}_{s0} we take only the conditions

$$(3.84) \quad \hat{T}_{s0}(\theta, 0) = -\frac{c_{i0}(\theta)}{\hat{m}_l} = -\frac{c_{tot}}{\hat{m}_l} \frac{1}{\hat{S}_0(\theta)}, \quad \frac{\partial \hat{T}_{s0}}{\partial Z} \Big|_{\xi=0} = \frac{\rho}{k\text{St}} \hat{S}'_0(\theta).$$

This finishes the analysis of regime iii, in which we observed that the buildup of impurities in the liquid phase causes enough supercooling to slow the interface down. At the final stages of this regime, that is, when $\theta \rightarrow +\infty$, we observe that at leading order the position of the interface tends to zero, and thus the interfacial concentration and temperature blow up. Therefore, we need to introduce regime iv to capture the behavior in that limit.

3.4. Asymptotic solutions in regime iv. Finally, we focus our attention on the late time part of the problem: regime iv. Again, we distinguish two layers: the outer layer I and the inner layer J. In the previous layers, we took D to be of order ϵ as this assumption was sufficient to decouple the diffusion of impurities in the solid from the remainder of the analysis. With this scaling, in regime iv we would need to consider an extra layer in the solid phase (between layers I and J) where we observe diffusion of impurities. For simplicity, and because this layer would only provide new information for c_s at the very end of the process, which is of small relevance to our analysis as discussed later, we take $D = \mathcal{O}(\epsilon^p)$ for some $p > 3$, which prevents diffusion of impurities from occurring in layer J. This assumption keeps the concentration profile stationary in both layers I and J and, despite the rescaling, does not affect the matching with previous layers.

3.4.1. Layer I. We consider first the outer layer I, using the rescalings shown in Figure 4. The problem is defined in $0 < z < 1$ by

$$(3.85a) \quad \frac{\partial \hat{c}_s}{\partial t} = \epsilon^{p+1} \hat{D} \frac{\partial^2 \hat{c}_s}{\partial z^2}, \quad \frac{\partial T_s}{\partial t} = \kappa \frac{\partial^2 T_s}{\partial z^2},$$

$$(3.85b) \quad \frac{\partial \hat{c}_s}{\partial z} = 0 \quad \text{and} \quad T_s = -1 \quad \text{at} \quad z = 1,$$

and appropriate matching conditions with layers J and F. At $\mathcal{O}(1)$, the problem is

$$(3.86a) \quad \frac{\partial \hat{c}_{s0}}{\partial t} = 0, \quad \frac{\partial T_{s0}}{\partial t} = \kappa \frac{\partial^2 T_{s0}}{\partial z^2},$$

$$(3.86b) \quad \frac{\partial \hat{c}_{s0}}{\partial z} = 0 \quad \text{and} \quad T_{s0} = -1 \quad \text{at} \quad z = 1.$$

In a similar way as we did before, we find that $c_s = \epsilon \hat{\alpha} c_i$. In section 3.4.3 we derive the matching conditions that complete the problem for T_{s0} , so we have

$$(3.87a) \quad \frac{\partial T_{s0}}{\partial t} = \kappa \frac{\partial^2 T_{s0}}{\partial z^2} \quad \text{in} \quad 0 < z < 1,$$

$$(3.87b) \quad \frac{\partial T_{s0}}{\partial z} = 0 \quad \text{at} \quad z = 0,$$

$$(3.87c) \quad T_{s0} = -1 \quad \text{at} \quad z = 1,$$

$$(3.87d) \quad T_{s0} = -1 + \frac{\operatorname{erf}\left(\frac{\lambda}{\sqrt{\kappa}}(1-z)\right)}{\operatorname{erf}\left(\frac{\lambda}{\sqrt{\kappa}}\right)} \quad \text{at} \quad t = t^* + \epsilon \tau^*.$$

Using separation of variables (as the problem is defined in the fixed domain $0 < z < 1$), we find

$$(3.88) \quad T_{s0} = -1 + \sum_{n=0}^{\infty} a_n e^{-\left(\frac{2n+1}{2}\pi\right)^2 \kappa(t-t^*-\epsilon\tau^*)} \cos\left(\frac{2n+1}{2}\pi z\right),$$

where the coefficients a_n are defined by

$$(3.89) \quad a_n = 2 \int_0^1 \frac{\operatorname{erf}\left(\frac{\lambda}{\sqrt{\kappa}}(1-z)\right)}{\operatorname{erf}\left(\frac{\lambda}{\sqrt{\kappa}}\right)} \cos\left(\frac{2n+1}{2}\pi z\right) dz.$$

3.4.2. Layer J. For the inner layer, J, we take the relevant scalings shown in Figure 4, and then rewrite the problem as

$$(3.90a) \quad \frac{\partial c_s}{\partial t} = \epsilon^{p-3} \hat{D} \frac{\partial^2 c_s}{\partial Z^2}, \quad \epsilon^4 \frac{\partial T_s}{\partial t} = \kappa \frac{\partial^2 T_s}{\partial Z^2}, \quad \epsilon^3 \frac{\partial \hat{c}_l}{\partial t} = \frac{\partial^2 \hat{c}_l}{\partial Z^2}, \quad \epsilon^4 \frac{\partial T_l}{\partial t} = \frac{\partial^2 T_l}{\partial Z^2},$$

$$(3.90b) \quad T_s = T_l, \quad c_s = \hat{\alpha} \hat{c}_l, \quad \hat{c}_l = -\hat{m}_l T_l,$$

$$\epsilon^4 \frac{\rho}{\operatorname{St}} \frac{d\hat{S}}{dt} = k \frac{\partial T_s}{\partial Z} - \frac{\partial T_l}{\partial Z}, \quad \epsilon^3 (1 - \epsilon \hat{\alpha}) \hat{c}_l \frac{d\hat{S}}{d\tau} = \epsilon^{p+1} \hat{D} \frac{\partial c_s}{\partial Z} - \frac{\partial \hat{c}_l}{\partial Z}$$

at the interface ($Z = \hat{S}(t)$), and

$$(3.90c) \quad \frac{\partial \hat{c}_l}{\partial Z} = 0 \quad \text{and} \quad \frac{\partial T_l}{\partial Z} = 0 \quad \text{at} \quad Z = 0.$$

At $\mathcal{O}(1)$, the problem reads

$$(3.91a) \quad \frac{\partial c_{s0}}{\partial t} = 0, \quad \frac{\partial^2 T_{s0}}{\partial Z^2} = 0, \quad \frac{\partial^2 \hat{c}_{l0}}{\partial Z^2} = 0, \quad \frac{\partial^2 T_{l0}}{\partial Z^2} = 0,$$

$$(3.91b) \quad T_{s0} = T_{l0}, \quad c_{s0} = \hat{a}\hat{c}_{l0}, \quad \hat{c}_{l0} = -\hat{m}_l T_{l0}, \quad \frac{\partial T_{s0}}{\partial Z} = \frac{\partial T_{l0}}{\partial Z}, \quad \frac{\partial \hat{c}_{l0}}{\partial Z} = 0$$

at the interface, and

$$(3.91c) \quad \frac{\partial \hat{c}_{l0}}{\partial Z} = 0 \quad \text{and} \quad \frac{\partial T_{l0}}{\partial Z} = 0 \quad \text{at } Z = 0.$$

The solution is then

$$(3.92) \quad c_{s0} = \hat{a}c_{i0}(\hat{S}_0^{-1}(Z)), \quad \hat{c}_{l0} = c_{i0}(t), \quad T_{s0} = -\frac{c_{i0}(t)}{\hat{m}_l}, \quad T_{l0} = -\frac{c_{i0}(t)}{\hat{m}_l},$$

so we will need to determine both $c_{i0}(t)$ and $\hat{S}_0(t)$. The first can be determined from the matching with (3.88), but we need to determine T_s up to $\mathcal{O}(\epsilon^2)$ first. The resulting problems are the same as for $\mathcal{O}(1)$, therefore, we find

$$(3.93) \quad T_s = -\frac{c_{i0}(t)}{\hat{m}_l} - \epsilon \frac{c_{i1}(t)}{\hat{m}_l} - \epsilon^2 \frac{c_{i2}(t)}{\hat{m}_l}.$$

In order to determine the position of the interface we need to determine $c_{l3}(t, Z)$ which gives $c_{l3} = \frac{1}{2}c'_{i0}(t)Z^2 + A_5(t)$, where $A_5(t)$ is a function of time that we do not need to determine for the purpose of our analysis. Then, the interface condition at $\mathcal{O}(\epsilon^3)$ gives, as in regime iii, that $c_{i0}(t)\hat{S}_0(t) = c_{tot}$, where the total concentration c_{tot} is the same as in regime iii.

3.4.3. Matching of the solutions. In this regime we only need to match T_s in layer I both with layers J and F to determine the boundary and initial conditions, respectively. We start matching the inner layer J with the outer layer I. Taking one term in the outer solution and three terms in the inner solution we find

$$(3.94) \quad (3ti)(1to) = T_{s0}(t, 0) + \epsilon^2 Z \left. \frac{\partial T_{s0}}{\partial z} \right|_{z=0}, \quad (1to)(3ti) = -\frac{c_{i0}(t)}{\hat{m}_l},$$

and thus we conclude

$$(3.95) \quad \left. \frac{\partial T_{s0}}{\partial z} \right|_{z=0} = 0, \quad c_{i0}(t) = -\hat{m}_l T_{s0}(t, 0),$$

where the first condition is the boundary condition at $z = 0$ that we need to solve the problem in layer I while the second determines $c_{i0}(t)$.

Finally, we match the outer layer in time I with the inner layer F. As the inner solution does not depend on time, the matching is trivial and we find

$$(3.96) \quad T_{s0}(t^* + \epsilon\tau^*, z) = -1 + \frac{\operatorname{erf}\left(\frac{\lambda}{\sqrt{\kappa}}(1-z)\right)}{\operatorname{erf}\left(\frac{\lambda}{\sqrt{\kappa}}\right)},$$

which is the initial condition for the problem in layer I. Therefore, we have completed the problem for T_{s0} in layer I.

This concludes the analysis of the last regime of the problem, as the solutions found here hold up to the limit $t \rightarrow +\infty$. Therefore, bringing together the solutions found in each of the four time regimes, we can describe, at leading order, the behavior of the system (2.5) for $t \in [0, +\infty)$.

3.5. Summary of asymptotic solutions. To summarize, our analysis has revealed four different time regimes within which we distinguish significantly different behaviors of the solutions. In all four regimes, we found that the impurities in the solid diffuse so slowly that the diffusion process in the solid can be neglected. In this section we provide the leading order solutions in each layer, rewritten in terms of the original dimensionless parameters (i.e., before rescaling). Remember that we defined the small parameter $\epsilon = \text{Le}^{-1}$. We do not provide a composite asymptotic solution given that it would require us to solve each layer up to $\mathcal{O}(\epsilon^2)$.

In regime i, which is at the beginning of the process, the time scale is $\mathcal{O}(1)$. This regime has two outer layers, one in the liquid and one in the solid, and a transition layer around the solidification front. In the outer layer in the solid ($z > S(t)$, layer A), we have

$$(3.97a) \quad c_s \approx \alpha c_i \quad \text{and} \quad T_s \approx -1 + \frac{\text{erf}\left(\frac{1-z}{2\sqrt{\kappa t}}\right)}{\text{erf}\left(\frac{\lambda}{\sqrt{\kappa}}\right)}$$

in the transition layer ($z = S(t)$, layer B), we have

$$(3.97b) \quad \begin{aligned} c_s &\approx \alpha c_i, \quad T_s \approx -\frac{\rho}{k\text{St}} \frac{\lambda}{\sqrt{t}}(z - S(t)) - \frac{c_i}{m_l}, \\ c_l &\approx c_i \exp\left(\frac{\lambda}{\sqrt{t}} \text{Le}(z - S(t))\right), \quad T_l \approx -\frac{c_i}{m_l}; \end{aligned}$$

and in the outer layer in the liquid ($z < S(t)$, layer C), we have

$$(3.97c) \quad c_l \approx c_0, \quad T_l \approx \left(T_0 + \frac{c_i}{m_l}\right) \frac{4}{\pi} \sum_{n=0}^{\infty} \frac{(-1)^n}{2n+1} e^{-(\frac{2n+1}{2}\pi)^2 t} \cos\left(\frac{2n+1}{2}\pi \frac{z}{S(t)}\right) - \frac{c_i}{m_l},$$

where

$$(3.97d) \quad S(t) \approx 1 - 2\lambda\sqrt{t} \quad \text{and} \quad c_i \approx \frac{2\lambda^2 c_0}{2\lambda^2 \alpha + \text{Le}^{-1}},$$

and the constant λ is found from (3.33). Remember that for T_l in layer C, apart from the asymptotic expansion in the limit of large Lewis number, we have used an asymptotic expansion in the limit of small λ (which is equivalent to small Stefan number), so the solution provided is the leading order term in λ . In this regime, the system is driven by the thermal problem which has the self-similar behavior of a one-phase Stefan problem, with the classic \sqrt{t} motion of the interface [4]. This is because, at early times, due to the small supercooling the two solidification fronts do not interact significantly. For the impurity transport, there is a “snow plough” effect due to the rejection of impurities from the solid into the liquid, resulting in a buildup of impurities in a thin layer of size $\mathcal{O}(\epsilon)$ in the liquid phase adjacent to the interface.

Once the two fronts are within a distance $\mathcal{O}(\epsilon)$ from one another, they begin to notice the other, since the impurities can no longer diffuse away. This corresponds to regime ii, where the time scale is $\mathcal{O}(\epsilon)$ around the critical time $t = t^*$. We distinguish two layers: the outer layer D and the inner layer E. In the outer layer D in the solid ($z > 0$), the solutions are

$$(3.98a) \quad c_s \approx \alpha c_i \quad \text{and} \quad T_s \approx -1 + \frac{\text{erf}\left(\frac{\lambda}{\sqrt{\kappa}}(1-z)\right)}{\text{erf}\left(\frac{\lambda}{\sqrt{\kappa}}\right)},$$

while in the inner layer E around the origin, with the solid phase in $z > S(t)$ and the liquid in $z < S(t)$, we have

(3.98b)

$$\begin{aligned}
 c_s &\approx \alpha c_i \sum_{n=1}^{\infty} n \left[\exp(-2\lambda^2 \text{Le } n(n-1)z) + \exp(-2\lambda^2 \text{Le } n(n+1)z) \right], \\
 T_s &\approx -2\lambda^2 \frac{\rho}{k\text{St}} (z - S(t)) \\
 &\quad - \frac{c_i}{m_l} \sum_{n=1}^{\infty} n \left[\exp(-2\lambda^2 \text{Le } n(n-1)S(t)) + \exp(-2\lambda^2 \text{Le } n(n+1)S(t)) \right], \\
 c_l &\approx c_i \sum_{n=1}^{\infty} n \left[\exp(2\lambda^2 \text{Le } n(z - nS(t))) + \exp(2\lambda^2 \text{Le } n(-z - nS(t))) \right], \\
 T_l &\approx -\frac{c_i}{m_l} \sum_{n=1}^{\infty} n \left[\exp(-2\lambda^2 \text{Le } n(n-1)S(t)) + \exp(-2\lambda^2 \text{Le } n(n+1)S(t)) \right],
 \end{aligned}$$

where

$$(3.98c) \quad S(t) \approx -2\lambda^2 (t - t^* - \tau^*), \quad t^* = \frac{1}{4\lambda^2}, \quad \text{and} \quad \tau^* = \frac{k\text{St}}{\rho} \frac{1}{8\lambda^4} \frac{c_i}{m_l},$$

and remember that the given value for τ^* is the leading order term in the small λ expansion. The solutions show a buildup of concentration of impurities in the liquid, due to the interaction between the fronts. At this small time scale, the temperature in the solid remains constant (at leading order), and we find that the motion of the interface is linear. The temperature in the liquid is homogeneous and equal to the supercooling temperature at the interface. This behavior is explained by the fact that the buildup of impurities is not large enough to cause significant supercooling and, therefore, does not affect the temperature in the solid nor the motion of the interface.

In regime iii, the two fronts are within a distance $\mathcal{O}(\epsilon^{\frac{4}{3}})$ from one another. The time scale is of $\mathcal{O}(\epsilon^{\frac{4}{3}})$ around the critical time $t = t^* + \tau^*$. We distinguish three layers: an outer layer F in the solid, an inner layer G of size $\mathcal{O}(\epsilon^{\frac{2}{3}})$, and an inner layer H of size $\mathcal{O}(\epsilon^{\frac{4}{3}})$, both around the origin. In the outer layer F ($z > 0$), we have

$$(3.99a) \quad c_s \approx \alpha c_i \quad \text{and} \quad T_s \approx -1 + \frac{\text{erf}\left(\frac{\lambda}{\sqrt{\kappa}}(1-z)\right)}{\text{erf}\left(\frac{\lambda}{\sqrt{\kappa}}\right)};$$

in the inner layer G, we have

$$(3.99b) \quad c_s \approx \alpha c_i, \\
 T_s \approx -2\lambda^2 \frac{\rho}{k\text{St}} z + \frac{c_{tot}}{m_l} \int_{-\infty}^{t-t^*-\tau^*} \frac{S'(s)}{S(s)^2} \text{erfc}\left(\frac{z}{2\sqrt{\kappa}\sqrt{t-t^*-\tau^*-s}}\right) ds;$$

and in the inner layer H ($z > S(t)$ for the solid and $z < S(t)$ for the liquid), we have

$$(3.99c) \quad c_s \approx \frac{\alpha c_{tot}}{z}, \quad T_s \approx -\frac{1}{m_l} \frac{c_{tot}}{S(t)}, \quad c_l \approx \frac{c_{tot}}{S(t)}, \quad T_l \approx -\frac{1}{m_l} \frac{c_{tot}}{S(t)},$$

where

$$(3.99d) \quad c_{tot} = \frac{c_0}{2\lambda^2 \alpha \text{Le} + 1},$$

and $S(t)$ is the solution to the integro-differential equation (3.65). Given that we can eliminate all the parameters from the problem, we can use the numerical solution of the parameter-free problem (3.57) shown in Figure 6 and then rescale it to obtain the solution to the problem (3.56). Both temperature and concentration fields in the liquid are homogeneous at leading order, since the length scale is much smaller than the diffusive length scale. The concentration evolves so that mass is conserved in the shrinking liquid domain, and temperature evolves to preserve thermodynamic equilibrium. The concentration of impurities in the liquid is now large enough to cause significant supercooling, and the temperature gradient in the solid near the interface decreases as a result, causing the inward motion of the solidification fronts to slow down.

In regime iv, the final temporal regime, the time scale is $\mathcal{O}(1)$ and the fronts are within a distance of $\mathcal{O}(\epsilon^2)$. We distinguish an outer layer I and an inner layer J of $\mathcal{O}(\epsilon^2)$. In the outer layer, we have

$$(3.100a) \quad c_s \approx \alpha c_i, \quad T_s \approx -1 + \sum_{n=0}^{\infty} a_n e^{-\left(\frac{2n+1}{2}\pi\right)^2 \kappa(t-t^*-\tau^*)},$$

while in the inner layer ($z > S(t)$ for the solid and $z < S(t)$ for the liquid), we have

$$(3.100b) \quad c_s \approx \frac{\alpha C_{tot}}{z}, \quad T_s \approx -1 + \sum_{n=0}^{\infty} a_n e^{-\left(\frac{2n+1}{2}\pi\right)^2 \kappa(t-t^*-\tau^*)},$$

$$(3.100c) \quad c_l \approx m_l \left(1 - \sum_{n=0}^{\infty} a_n e^{-\left(\frac{2n+1}{2}\pi\right)^2 \kappa(t-t^*-\tau^*)} \right), \quad T_l \approx -1 + \sum_{n=0}^{\infty} a_n e^{-\left(\frac{2n+1}{2}\pi\right)^2 \kappa(t-t^*-\tau^*)},$$

where

$$(3.100d) \quad S(t) \approx \frac{C_{tot}}{m_l} \left(1 - \sum_{n=0}^{\infty} a_n e^{-\left(\frac{2n+1}{2}\pi\right)^2 \kappa(t-t^*-\tau^*)} \right)^{-1},$$

and the coefficients a_n are as given in (3.89). As in regime iii, we observe that the temperature and concentration profiles in the liquid are homogeneous and evolve in thermodynamic equilibrium jointly with the temperature in the solid which now decays to the temperature at the boundary. The interface position evolves so that the total concentration of impurities in the liquid is conserved.

4. Comparison with numerical simulations and experimental data. In order to validate the asymptotic solutions, we compare them to numerical simulations of the full problem (2.3) obtained via a finite volume scheme [23]. We also compare our solutions to experimental data.

4.1. Numerical scheme. In order to solve the problem (2.3) numerically we choose a fixed boundary scheme, similar to those described in [10, 41]. We rescale the solid and liquid domains so they have fixed boundaries. Because the Péclet number of the impurity equations ranges from large in the beginning to small at the end, extra care must be taken in order to avoid numerical instabilities. Therefore, we use a finite volume scheme with a TVD discretization for the advection term. We implement the scheme in MATLAB using the finite volume toolbox FVToolbox [9].

We introduce the variables $x = \frac{z-S(t)}{1-S(t)}$ for the solid phase and $y = \frac{z}{S(t)}$ for the liquid phase, both of which range from 0 to 1. We define the following quantities

$$(4.1) \quad \begin{aligned} \phi_1(t, x) &= [1 - S(t)]c_s(t, x), \\ \phi_2(t, x) &= [1 - S(t)]T_s(t, x), \\ \phi_3(t, y) &= S(t)c_l(t, y), \\ \phi_4(t, y) &= S(t)T_l(t, y), \end{aligned}$$

so we can rewrite the system (2.3) in conservation form. In the solid phase $x \in (0, 1)$, we have

$$(4.2a) \quad \frac{\partial \phi_1}{\partial t} + \frac{\partial}{\partial x} \left(-\frac{S'(t)}{1-S(t)}(1-x)\phi_1 - \frac{D}{\text{Le}(1-S(t))^2} \frac{\partial \phi_1}{\partial x} \right) = 0,$$

$$(4.2b) \quad \frac{\partial \phi_2}{\partial t} + \frac{\partial}{\partial x} \left(-\frac{S'(t)}{1-S(t)}(1-x)\phi_2 - \frac{\kappa}{1-S(t)^2} \frac{\partial \phi_2}{\partial x} \right) = 0;$$

in the liquid phase $y \in (0, 1)$, we have

$$(4.2c) \quad \frac{\partial \phi_3}{\partial t} + \frac{\partial}{\partial y} \left(-\frac{S'(t)}{S(t)}y\phi_3 - \frac{1}{\text{Le}S(t)^2} \frac{\partial \phi_3}{\partial y} \right) = 0,$$

$$(4.2d) \quad \frac{\partial \phi_4}{\partial t} + \frac{\partial}{\partial y} \left(-\frac{S'(t)}{S(t)}y\phi_4 - \frac{1}{S(t)^2} \frac{\partial \phi_4}{\partial y} \right) = 0;$$

at the interface (given by $x = 0$ and $y = 1$), we have

$$(4.2e) \quad S(t)\phi_2 = (1 - S(t))\phi_4,$$

$$(4.2f) \quad S(t)\phi_1 = \alpha(1 - S(t))\phi_3,$$

$$(4.2g) \quad \phi_3 = -m_l\phi_4,$$

$$(4.2h) \quad \frac{\rho}{\text{St}} \frac{dS}{dt} = \frac{k}{(1-S(t))^2} \frac{\partial \phi_2}{\partial x} - \frac{1}{S(t)^2} \frac{\partial \phi_4}{\partial y},$$

$$(4.2i) \quad -\frac{S'(t)}{1-S(t)}\phi_1 - \frac{D}{\text{Le}(1-S(t))^2} \frac{\partial \phi_1}{\partial x} = -\frac{S'(t)}{S(t)}\phi_3 - \frac{1}{\text{Le}S(t)^2} \frac{\partial \phi_3}{\partial y};$$

the boundary conditions are

$$(4.2j) \quad \frac{\partial \phi_1}{\partial x} = 0 \quad \text{and} \quad \phi_2 = -(1 - S(t)) \quad \text{at} \quad x = 1, \quad \frac{\partial \phi_3}{\partial y} = 0 \quad \text{and} \quad \frac{\partial \phi_4}{\partial y} = 0 \quad \text{at} \quad y = 0,$$

and we prescribe appropriate initial conditions for ϕ_1 , ϕ_2 , ϕ_3 , ϕ_4 , and S .

Since α is very small, we take $\alpha = 0$ and therefore we neglect the impurities in the solid, considering only impurities in the liquid when performing our simulations. This reduces the condition (4.2i) to a no-flux condition and removes (4.2a) and (4.2f) from the system. At each time step, we iterate using a relaxation scheme until convergence. At the $(k+1)$ th iteration, knowing the values of the k th iteration ϕ_2^k , ϕ_3^k , ϕ_4^k , S^k , and V^k , and the values at the previous time step ϕ_2^* , ϕ_3^* , ϕ_4^* , and S^* , we proceed in the following order:

1. Calculate ϕ_2^{k+1} , ϕ_3^{k+1} , and ϕ_4^{k+1} from (4.2b)–(4.2d) and the boundary conditions (4.2e), (4.2g), and (4.2i). We use the values of ϕ_3^k , S^k , and V^k at the previous iteration for the calculations.

2. Use (4.2h) to calculate the variation in velocity between iterations k and $k+1$, using the new values of ϕ_2^{k+1} and ϕ_4^{k+1} and the old value of S^k :

$$\Delta V^{k+1} = \frac{\text{St}}{\rho} \left(\frac{k}{(1-S^k)^2} \frac{\partial \phi_2^{k+1}}{\partial x} - \frac{1}{(S^k)^2} \frac{\partial \phi_4^{k+1}}{\partial y} \right) - V^k.$$

3. Calculate the new velocity using a relaxation coefficient ω as $V^{k+1} = V^k + \omega \Delta V^{k+1}$.
4. Update the position of the interface with the new velocity and the position of the interface at the previous time step. That is, $S^{k+1} = S^* + \Delta t V^{k+1}$.

We keep iterating until $|\frac{\Delta V^{k+1}}{V^{k+1}}| < \delta$, where δ is a prescribed tolerance. Then we can move to the next time step and start iterating again.

4.2. Comparison of asymptotic and numerical results. When performing our simulations, we set $\text{St} = 0.77$, $\text{Le} = 100$, $\rho = 1$, $c_p = 1$, $k = 0.36$, $m_l = 100$, $c_0 = 0.01$, $T_0 = 0$, which are representative of metallurgical grade silicon. We take $N_s = 5 \cdot 10^3$ grid points in the solid phase, $N_l = 10^4$ grid points in the liquid phase, and an initial time step of $\Delta t = 10^{-4}$. For the relaxation iterations, we take a relaxation parameter $\omega = 0.1$ and a tolerance of $\delta = 0.01$. To help convergence, if one time step takes more than 100 iterations before converging and the time step is larger than 10^{-5} we halve the time step. This algorithm is capable of solving the full problem with a total mass variation smaller than 0.01%.

The comparison between our asymptotic solutions and numerical simulations is shown in Figure 8. Based on the good agreement with the asymptotic solutions, we believe that the asymptotics accurately describe the true dynamics of the system, even as the fronts approach closely. In Figure 8(a) we plot the position of the interface, observing self-similar-like behavior for $t < t^* = 2.2294$, while for $t > t^*$ we observe exponential decay toward the final position of the interface, determined by $c_{tot} m_l^{-1} = 9.57 \cdot 10^{-5}$. In Figure 8(b) we plot the concentration in the liquid side of the interface. In regime i the concentration is constant until near t^* (regime ii), when the buildup of impurities becomes noticeable. For $t > t^*$, the buildup of impurities continues, with the concentration tending exponentially to a concentration $m_l = 100$. In Figures 8(c) and 8(d) we show the same comparison for the solution in regime iii (solid blue line) and the solutions in regimes ii and iv (dashed black lines) to show as well the matching between these three layers. As discussed earlier, we do not provide composite solutions as it would require us to calculate solutions up to $\mathcal{O}(\epsilon^2)$ in each layer, so the plotting domain for each regime in the plot is merely for illustrative purposes. Figures 8(e) and 8(f) show the comparison between asymptotic and numerical solutions for the temperature profiles in the solid phase and concentration profiles in the liquid phase (as time evolves, curves go from right to left). We observe good agreement as well between the asymptotic approximations and numerical simulations.

Finally, in Figure 9 we show the concentration of impurities on the liquid side of the interface as a function of time for different values of the Stefan and Lewis numbers, and we observe that the qualitative behavior is the same for both parameter sweeps. In particular, we notice that a decrease of St causes the system to cool at a slower rate and hence the solidification process happens more slowly. On the other hand, an increase of Le (which corresponds to a decrease of ϵ), results in a larger final concentration m_l , as from our asymptotic scalings we set m_l to scale with Le . We find also, even though it cannot be appreciated in the plot, that an increase of Le results in a quicker transition as regimes ii and iii are of size $\mathcal{O}(\epsilon)$ and $\mathcal{O}(\epsilon^{\frac{4}{3}})$, respectively.

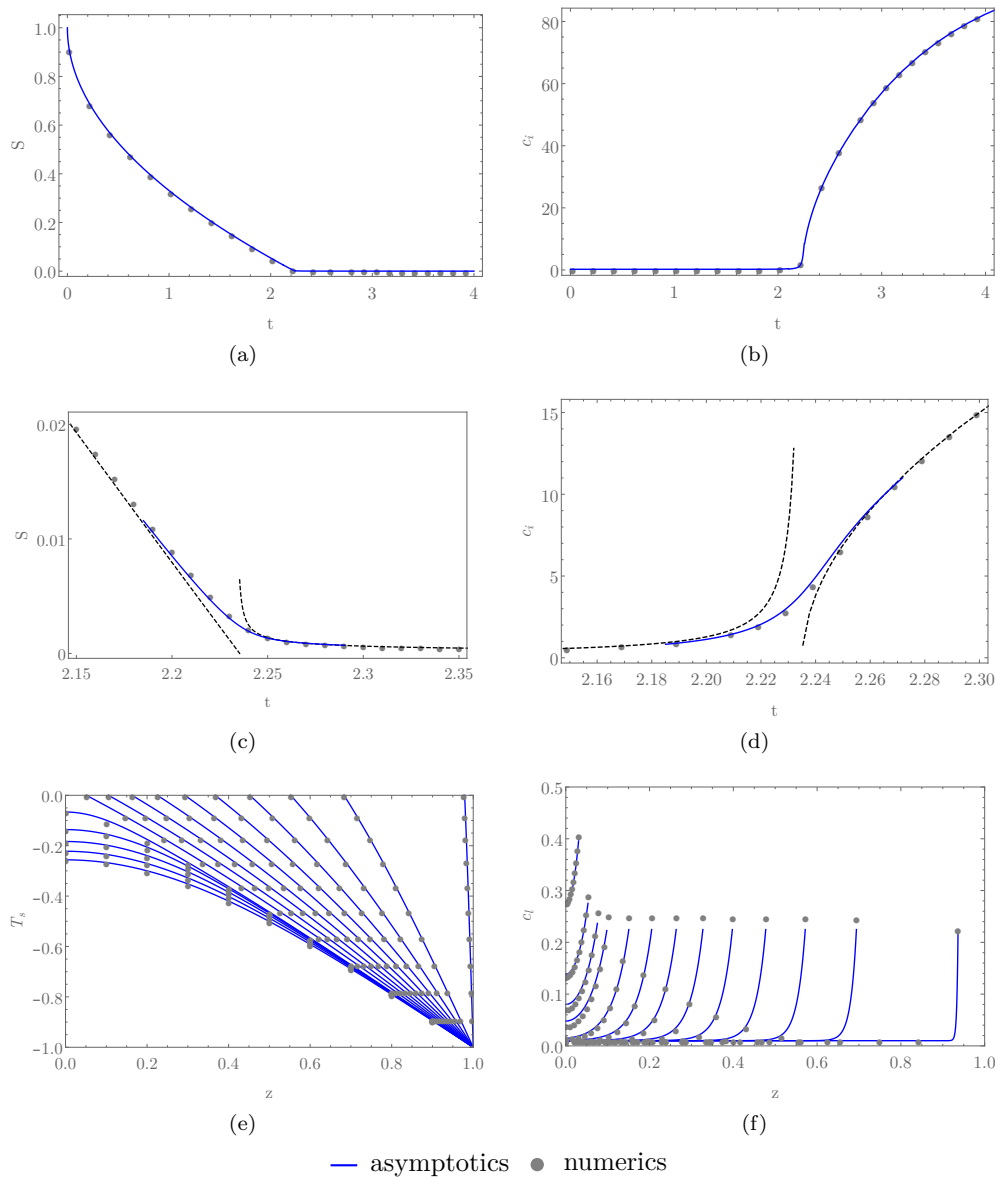


FIG. 8. Comparison of the analytical and numerical solution of (a) the interface position and (b) the concentration of impurities on the liquid side of the interface against time. Figures (c) and (d) show the zoom in regime iii (solid blue line) and how it matches with the solutions in regimes ii and iv (dashed black line). Finally, in (e) we show the temperature profiles in the solid and in (f) the concentration profiles in the liquid for different times. As time goes by, the curves go right to left.

4.3. Comparison with experimental results. As mentioned in section 1, an application which motivates this work is the casting of metallurgical grade silicon, and we now compare our results with experimental data of the casting of 99% pure silicon over a water cooled copper plate. These experimental data were provided by Elkem. In order to obtain the data, after the cast has cooled down, it is sliced into parts and treated in order to take the measurements on the internal faces of the slice. Grain

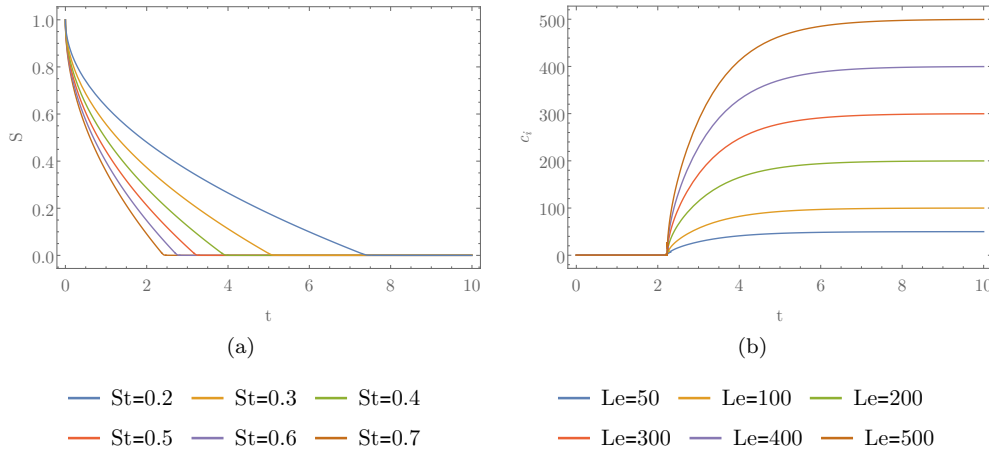


FIG. 9. Asymptotic solutions of the concentration of impurities on the liquid side of the interface against time for different values of (a) Stefan number St (where $St = 0.2$ is the rightmost curve and $St = 0.7$ the leftmost curve) and (b) Lewis number Le (where $Le = 50$ is the bottom curve and $Le = 500$ the top curve).

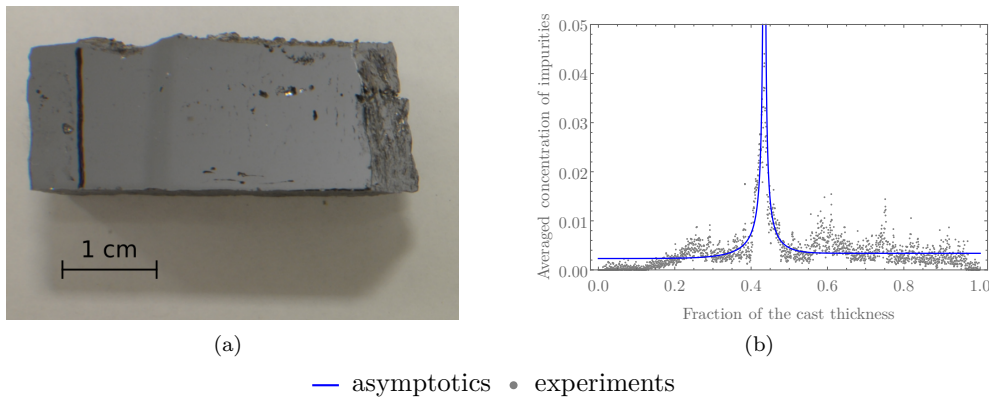


FIG. 10. (a) Picture of the sample used for the experimental data (imaged provided by Elkem). The experiment corresponds to a 14 mm silicon cast over a water cooled copper plate. The data are taken at a given central section of the cast which has been polished and chemically treated in order to take the measurements. (b) Comparison of the asymptotic solution and experimental data for the concentration in the solid phase. The experimental data have been provided by Elkem. For the asymptotic solution we used parameter values $c_0 = 0.01$, $\mu_r = 17$, $\mu_l = 10$, $\alpha = 0.03$, and $z_0 = 0.43$.

size, pore size, and impurity concentration are then recorded. These magnitudes are averaged over a certain width at every cross section, so the output data are recorded against the thickness direction variable. An image of the measured sample is shown in Figure 10(a). We are interested in measurements of the (cross-section averaged) concentration of impurities in the solid against the thickness of the cast. These data can be immediately compared to c_s , which we have found will not depend on time (to leading order). As the cast thickness is much smaller than its width, and the impurity concentration is averaged over a few centimetres of cross section, our planar model is a reasonable match to the experimental configuration.

In Figure 10(b), we plot the asymptotic solution and the experimental data. Due to scale, in the experimental data we only resolve regimes i and ii. The corresponding composite asymptotic solution for both regimes (at leading order) is

$$(4.3) \quad c_s(z) \approx \frac{\alpha\mu}{\alpha\mu + 1} c_0 \sum_{n=1}^{\infty} n \left(e^{-\mu(n+1)nz} + e^{-\mu n(n-1)z} \right),$$

where $\mu = 2\lambda^2 Le$. Thus, the concentration profile depends only on three dimensionless parameters, μ , α , and c_0 .

From the experimental data, we observe the concentration profiles produced by two solidification fronts which are not symmetric, and eventually meet at a point z_0 of the cast. To match this with asymptotic solutions, we assume each side of the plot can be modeled by (4.3) combining $c_s(z - z_0)$ and $c_s(z_0 - z)$, both with the same parameters α and c_0 (as these are given by the material properties). On the other hand, the parameter μ depends on the cooling rate which has different values at the top and at the bottom of the cast due to the different heat transfer mechanisms. However, we know that both fronts meet at the same time, and at $z = z_0$, therefore, we have the relation

$$(4.4) \quad \mu_l = \left(\frac{z_0}{1 - z_0} \right)^2 \mu_r,$$

where subscripts r and l denote the right and left side of the central cross section $z = z_0$. We use reasonable parameter values for our problem to compare the asymptotic solution (4.3) with the experimental data. Using the parameter values $c_0 = 0.01$, $\mu_r = 17$, $\mu_l = 10$, $\alpha = 0.03$ and $z_0 = 0.43$, we obtain the asymptotic solution shown in Figure 10(b). Notice that these values of μ_l , μ_r , and α are significantly different than the ones used in the numerical simulations. Given the simplicity of our model, we treat these parameters as effective coefficients that can be determined experimentally for a given physical setup. The asymptotic solution captures the rapid growth of the concentration near the region where the solidification fronts meet, and the constant concentration outside of this region. The noise in the data is caused by the bubbles and pores of the cast, as impurities tend to aggregate around them. In spite of these complications, the asymptotic solutions show good qualitative agreement with the experimental data.

5. Discussion. We have considered an asymptotic analysis for the extended Stefan problem modeling the solidification of a binary alloy in a finite slab. We distinguished four different time regimes, each featuring multiple spatial layers. The dynamics at the beginning of the process are akin to those of the classical one-phase classical Stefan problem (for which there exist self-similar solutions). The impurities are rejected from the solid into the liquid and then diffuse away within a thin layer near the solidification front. The value of the concentration at the interface remains constant. When the two fronts move close to each other, the interaction between the fronts causes the concentration in the liquid to increase, since the rejected impurities can no longer diffuse away. As time increases, the concentration of impurities in the liquid phase becomes large enough to influence the temperature field, resulting in a slowing of the solidification front motion (so that the fronts do not collide). In the late stages of the process, the system is driven by cooling of the solid towards the uniform state given by the thermal boundary value. These asymptotic solutions are shown to agree with numerical simulations and experimental data.

We conclude that supercooling plays a crucial role in the time evolution of the system as the fronts approach one another and the impurities build up. It is also noteworthy that the transition between the two main regimes occurs in two stages. In the first stage, there is a quick buildup of impurities in the liquid, yet the interface continues to move as for earlier time. In the second stage, a significant change in the solidification front occurs as it slows down as the impurity buildup has modified the thermal properties of the system. We also find that the cooling rate λ has a large impact for the late-time dynamics, particularly in the concentration fields, as it determines the value of c_{tot} .

One potential industrial application of our analysis would be an improved understanding of the casting process for materials such as silicon. We have shown that the distribution of impurities in the final solidified slab is determined by the cooling rate, λ , the initial impurity concentration, c_0 , the segregation coefficient, α , and the Lewis number, Le . The latter two are physical parameters which depend on the material and the impurities and, hence, cannot be controlled. The parameter c_0 is also normally restricted by the specific application, so the only control parameter is λ . The parameter $\mu = 2\lambda^2 Le$ defines the thickness of the impurity buildup layer, therefore λ influences both the concentration far from the central layer and the thickness of the layer of impurities. As λ depends on the heat exchange of each boundary, the cooling conditions applied to the cast could, in principle, be used to control the profile of the concentration of impurities in the solid slab. Moreover, the experimental data suggest that the thickness of this layer correlates with the thickness of the equiaxed grain layer, therefore the results presented here could be used to obtain a semiempirical estimation of the thickness of the equiaxed layer. These could be an alternative to the several analyses of the columnar to equiaxed transition existing in the literature (see [11, 12, 16] for a few examples). For more information on the topic, we refer the reader to the book [8].

Possible extensions of this work would be to consider two-dimensional radially symmetric (cylindrical) and three-dimensional (spherical) geometries, thereby extending the work presented in [10, 27, 33] to an extended Stefan problem for binary alloys in these geometries. Another extension would be to consider arbitrary two- and three-dimensional geometries to generalize the results presented in [25, 26]. One might also consider the role of nonuniform boundaries, such as configurations where the molten material is placed on a bed of fines, resulting in initially uneven penetration of the solidification front at small times as discussed in [2]. In these configurations one could study as well the differences in the heat exchange mechanisms when introducing a layer of fines. Finally, the stability of the solutions for each regime could be studied, which may potentially lead to a better understanding of the columnar to equiaxed transition. Identifying particular instabilities possible on each time scale might provide a better understanding of the grain formation process.

Acknowledgments. We thank A. Autruffe, K. Hildal, B. Kroka, and A. Valderhaug for useful discussions. We would like also to thank Prof. S. D. Howison and Prof. A. A. Lacey for their insightful comments on this work.

REFERENCES

- [1] D. N. DE G. ALLEN AND R. T. SEVERN, *The application of relaxation methods to the solution of non-elliptic partial differential equations: II. The solidification of liquids*, Quart. J. Mech. Appl. Math., 5 (1952), pp. 447–454.
- [2] G. P. BENHAM, K. HILDAL, C. P. PLEASE, AND R. A. VAN GORDER, *Penetration of molten silicon into a bed of fines*, Int. Commun. Heat Mass Transf., 75 (2016), pp. 323–327.

- [3] G. P. BENHAM, K. HILDAL, C. P. PLEASE, AND R. A. VAN GORDER, *Solidification of silicon in a one-dimensional slab and a two-dimensional wedge*, Int. J. Heat Mass Transf., 98 (2016), pp. 530–540.
- [4] F. BROSA PLANELLA, C. P. PLEASE, AND R. A. VAN GORDER, *Instability in the self-similar motion of a planar solidification front*, IMA J. Appl. Math., 83 (2018), pp. 106–130.
- [5] W. D. CALLISTER AND D. G. RETHWISCH, *Materials Science and Engineering*, Vol. 5, Wiley, New York, 2011.
- [6] J. CRANK AND R. S. GUPTA, *Isotherm migration method in two dimensions*, Int. J. Heat Mass Transf., 18 (1975), pp. 1101–1107.
- [7] A. B. CROWLEY, *Numerical solution of Stefan problems*, Int. J. Heat Mass Transf., 21 (1978), pp. 215–219.
- [8] G. B. DAVIS AND J. M. HILL, *A moving boundary problem for the sphere*, IMA J. Appl. Math., 29 (1982), pp. 99–111.
- [9] A. A. EFTEKHARI AND K. SCHÜLLER, *FVTool: A Finite Volume Toolbox for Matlab*, <https://doi.org/10.5281/zenodo.32745> (2015).
- [10] D. L. FELTHAM AND J. GARSIDE, *Analytical and numerical solutions describing the inward solidification of a binary melt*, Chem. Eng. Sci., 56 (2001), pp. 2357–2370.
- [11] S. C. FLOOD AND J. D. HUNT, *Columnar and equiaxed growth: I. A model of a columnar front with a temperature dependent velocity*, J. Crystal Growth, 82 (1987), pp. 543–551.
- [12] S. C. FLOOD AND J. D. HUNT, *Columnar and equiaxed growth: II. Equiaxed growth ahead of a columnar front*, J. Crystal Growth, 82 (1987), pp. 552–560.
- [13] J. M. HILL AND A. KUCERA, *Freezing a saturated liquid inside a sphere*, Int. J. Heat Mass Transf., 26 (1983), pp. 1631–1637.
- [14] J. M. HILL AND A. KUCERA, *The time to complete reaction or solidification of a sphere*, Chem. Eng. Sci., 38 (1983), pp. 1360–1362.
- [15] R. N. HILLS, D. E. LOPER, AND P. H. ROBERTS, *A thermodynamically consistent model of a mushy zone*, Quart. J. Mech. Appl. Math., 36 (1983), pp. 505–540.
- [16] J. D. HUNT, *Steady state columnar and equiaxed growth of dendrites and eutectic*, Mater. Sci. Eng., 65 (1984), pp. 75–83.
- [17] L. M. JIJI AND S. WEINBAUM, *Perturbation solutions for melting or freezing in annular regions initially not at the fusion temperature*, Int. J. Heat Mass Transf., 21 (1978), pp. 581–592.
- [18] J. R. KING, D. S. RILEY, AND A. M. WALLMAN, *Two-dimensional solidification in a corner*, R. Soc. Lond. Proc. A Math. Phys. Eng. Sci., 455 (1999), pp. 3449–3470.
- [19] O. KUBASCHEWSKI, *Iron-Binary Phase Diagrams*, Springer, Berlin, 1982.
- [20] A. KUCERA AND J. M. HILL, *On inward solidifying cylinders and spheres initially not at their fusion temperature*, Int. J. Nonlinear Mech., 21 (1986), pp. 73–82.
- [21] G. LAMÉ AND B. P. E. CLAPEYRON, *Mémoire sur la solidification par refroidissement d'un globe liquide*, Ann. Chim. Phys., 47 (1831), pp. 250–256.
- [22] A. LAZARIDIS, *A numerical solution of the multidimensional solidification (or melting) problem*, Int. J. Heat Mass Transf., 13 (1970), pp. 1459–1477.
- [23] R. J. LEVEQUE, *Finite Volume Methods for Hyperbolic Problems*, Vol. 31, Cambridge University Press, Cambridge, 2002.
- [24] F. LIU AND D. L. S. MCELWAIN, *A computationally efficient solution technique for moving-boundary problems in finite media*, IMA J. Appl. Math., 59 (1997), pp. 71–84.
- [25] S. W. MCCUE, J. R. KING, AND D. S. RILEY, *Extinction behaviour for two-dimensional inward-solidification problems*, R. Soc. Lond. Proc. A Math. Phys. Eng. Sci., 459 (2003), pp. 977–999.
- [26] S. W. MCCUE, J. R. KING, AND D. S. RILEY, *The extinction problem for three-dimensional inward solidification*, J. Engrg. Math., 52 (2005), pp. 389–409.
- [27] S. W. MCCUE, B. WU, AND J. M. HILL, *Classical two-phase Stefan problem for spheres*, R. Soc. Lond. Proc. A Math. Phys. Eng. Sci., 464 (2008), pp. 2055–2076.
- [28] J. R. OCKENDON, S. D. HOWISON, A. A. LACEY, AND A. B. MOVCHAN, *Applied Partial Differential Equations*, Oxford University Press, Oxford, 1999.
- [29] A. D. POLYANIN, *Handbook of Linear Partial Differential Equations for Engineers and Scientists*, CRC Press, Boca Raton, FL, 2001.
- [30] D. S. RILEY, F. T. SMITH, AND G. POOTS, *The inward solidification of spheres and circular cylinders*, Int. J. Heat Mass Transf., 17 (1974), pp. 1507–1516.
- [31] L. I. RUBINSTEIN, *The Stefan Problem*, Transl. Math. Monogr. 27, American Mathematical Society, Providence, RI, 1971.
- [32] M. S. SELIM AND R. C. SEAGRAVE, *Solution of moving-boundary transport problems in finite media by integral transforms. II. Problems with a cylindrical or spherical moving boundary*, Ind. Eng. Chem. Fund., 12 (1973), pp. 9–13.

- [33] A. M. SOWARD, *A unified approach to Stefan's problem for spheres and cylinders*, R. Soc. Lond. Proc. A Math. Phys. Eng. Sci., 373 (1980), pp. 131–147.
- [34] J. STAM AND R. SCHMIDT, *On the velocity of an implicit surface*, ACM Trans. Graph., 30 (2011), 21.
- [35] J. STEFAN, *Über die Theorie der Eisbildung*, Monatsh. Math., 1 (1890), pp. 1–6.
- [36] K. STEWARTSON AND R. T. WAECHTER, *On Stefan's problem for spheres*, R. Soc. Lond. Proc. A Math. Phys. Sci., 348 (1976), pp. 415–426.
- [37] L. C. TAO, *Generalized numerical solutions of freezing a saturated liquid in cylinders and spheres*, AIChE J., 13 (1967), pp. 165–169.
- [38] M. VAN DYKE, *Perturbation Methods in Fluid Mechanics*, Parabolic Press, Stanford, CA, 1975.
- [39] V. VOLLER AND M. CROSS, *Accurate solutions of moving boundary problems using the enthalpy method*, Int. J. Heat Mass Transf., 24 (1981), pp. 545–556.
- [40] A. M. WALLMAN, J. R. KING, AND D. S. RILEY, *Asymptotic and numerical solutions for the two-dimensional solidification of a liquid half-space*, R. Soc. Lond. Proc. A Math. Phys. Eng. Sci., 453 (1997), pp. 1397–1410.
- [41] G.-X. WANG, V. PRASAD, AND E. F. MATTHYS, *An interface-tracking numerical method for rapid planar solidification of binary alloys with application to microsegregation*, Mater. Sci. Eng. A, 225 (1997), pp. 47–58.
- [42] M. G. WORSTER, *Solidification of an alloy from a cooled boundary*, J. Fluid Mech., 167 (1986), pp. 481–501.
- [43] J. YANG, C.-Y. ZHAO, AND D. HUTCHINS, *Modelling the effect of binary phase composition on inward solidification of a particle*, Int. J. Heat Mass Transf., 55 (2012), pp. 6766–6774.